

Optimization of Standalone Hybrid Renewable Energy Systems Using Different Metaheuristic Techniques Considering Demand Side Management

Mohamed A. Hassanein¹, Mohamed A. Mohamed^{1,*}, Ahmed A. Hassan¹
¹Electrical Engineering Dep., Faculty of Engineering, Minia University, Minia, Egypt
* Corresponding Author: Email: dr.mohamed.abdelaziz@mu.edu.eg

ARTICLE INFO

Article history:

Received: 2 September 2024

Revised: 26 November 2024

Accepted: 25 February 2025

Keywords:

Isolated Microgrids

Demand Side Management (DSM)

Cost of Energy (COE)

Dummy Energy

Loss of Power Supply Probability (LPSP)

Optimization

ABSTRACT

This paper introduces an effective optimization program describing the techno-economic analysis of a standalone hybrid PV/wind turbine/diesel generator/battery bank storage energy system depending on real-time information and meteorological data of New Minia city located in Egypt. The optimum sizing of the proposed system has been determined by using various-metaheuristic algorithms in addition to effective strategies such as demand side management (DSM), load following (LF), cycle charging (CC) to minimize the cost of supplied energy (COE) constrained by the loss of power supply probability (LPSP) and amount of dummy energy, while increasing the reliability and efficiency of the proposed system. An advanced optimization algorithm based Salp Swarm Algorithm (SSA) in comparison with various-metaheuristic algorithms have been applied for designing the optimum size of isolated microgrid. The simulation results showed the optimal performance of the SSA algorithm over the other techniques.

1. Introduction

1.1. Motivation

In light of providing a clean, sustainable and developed environment that relies on the use of renewable energies (RE), many countries have sought to reclaim remote areas and build new residential cities to accommodate the population increase [1,2]. Many feasibility studies and planning were conducted on electrifying these remote cities from the electrical grid. It was found that the connection to the electrical grid is relatively costly and sometimes technically constrained [3-7]. In addition to climate change due to reliance on fossil fuels [8,9] like diesel, natural gas, coal, mazut and oil, which used as prime energy sources for electric power generation stations, transportation, and industries [10,11]. These fuels are exhaustible and cause environmental pollution due to the spread of greenhouse gases (GHGs) [12], especially CO₂ emissions. Accordingly, many countries began exploiting natural, free-cost, clean, green, reliable, and environment-friendly sources [13,14], such as bioenergy, heat pumping technologies (HPT), geothermal, tidal, green hydrogen (GH), hydropower (HP), ocean, PV, solar heating and cooling (SHC), solar paces, and wind energy, which are the best alternative sources to fossil fuels. The international agency of energy (IEA) suggested that over the period of 2023-2028, almost 3700 GW of additional renewable capacity will be added. By 2028, more than 42% of the world's power will come from renewable sources with an increase about 9.5% in PV and 6.1% in wind per year from 2020 to 2028 [15], which the two most promising energy resources employed in Egypt. The unpredictable nature of solar radiation and wind speed is the main challenge [16], which forbids their use as

individual power sources to feed microgrids. Therefore, this problem can be overcome by connecting the microgrid of RE sources to the main grid [17,18], as a two-way power flow [19], but connection with the grid is costly for this isolated area and sometimes technically constrained [20-22]. So, the recommended second way is to combine various renewable and traditional energy sources to develop an integrated hybrid RE system (IHRES) containing a storage system such as cell battery, FC, supercapacitors, flywheels (FWs), molten salt, hydroelectric pumped storage system (HPSS), and compressed air, in addition to a standby DG to provide more reliability and less cost-effective energy [23,24]. Therefore, this paper focalizes on determining the optimum size of each component in an isolated hybrid PV/WT/DG/battery energy system for cite of New Minia city located in Egypt. Depending on real-time information and meteorological data for the global horizontal irradiation (GHI) and wind speed distributions at height of 50m as shown in Figure 1 and Figure 2, respectively.

1.2. Literature Review on Sizing Methods and Optimization Techniques

Several studies have been introduced for techno-economic sizing of standalone HRES for remote areas. There are many configurations for hybrid energy systems, most of these depend mainly on energy from solar PV panels and WT with a standby battery bank storage system or internal combustion DG [25-27], Others depend on different renewable sources [28,29], where the surplus of energy may be stored in different energy storing devices [30,31]. The sizing methods can be distinguished as follows:

1.2.1. Sizing of Hybrid Energy System Using Software Tools

Commercial software used as applications depending on C++ programming language with windows platforms such as:

Canadian software “RET Screen” which developed in 1998 for sizing of energy systems with considering optimization and technical, financial, environmental analysis, system losses, power efficiency and cogeneration projects [32]. With the last update became multi-agent tool for sizing of solar PV panels, WTs, DG and battery bank integrated system based on energy production, total net present costs and reduction of greenhouse gas which reaches more than 99% depending on RE resources [33].

iHOGA (Improved Hybrid Optimization by Genetic Algorithm) software is a multi-agent tool deals with renewable and conventional resources such as PV, WT, FC, hydroelectric turbines, battery bank storage system and internal combustion DGs, where it used to optimize sizing of integrated energy system of PV/WT/DG/Battery for a house in Paris by reducing emissions of greenhouse gases specially CO₂ by 73.8% and unmet load by 68% [34].

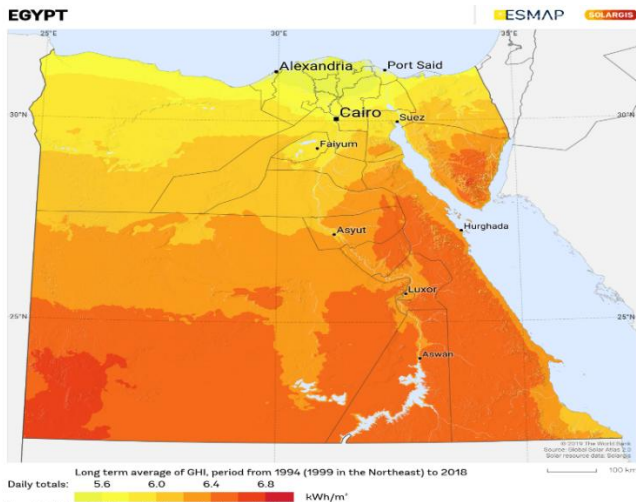


Figure 1: The global horizontal irradiation (GHI) map of Egypt

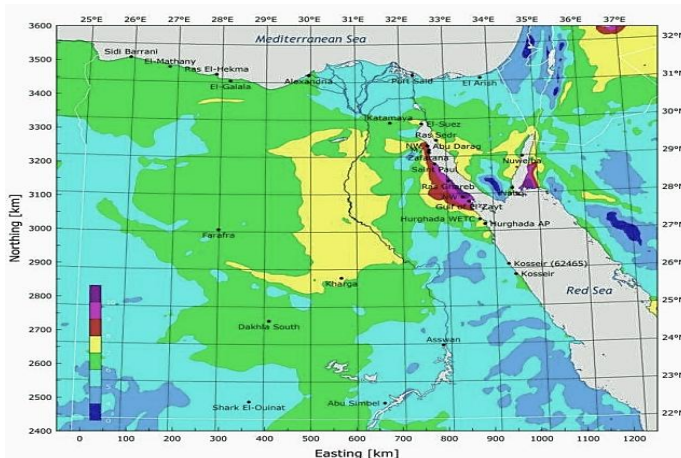


Figure 2: The wind speed distribution map of Egypt

Hybrid2 software was developed in 1996 by laboratory of RE research (RERL) of the Massachusetts university [35], which gives

an analysis on hybrid energy system containing PV, WT, battery bank storage system, power converters and dummy energy with high performance [36], where it used for sizing PV/WT/FC hybrid system in Chicago [37].

HOMER (Hybrid Optimization Model for Electric Renewable) software has developed for both grid connected and isolated grid ways in 1993 by the laboratory of national RE (NREL) [38]. It is used in Shiraz for optimum sizing of hybrid energy system based on PV, WT, DG and storage system of battery with minimum COE between 9,3 to 12,6 c/kWh and less percentage amount of dioxide carbon, where the RE generated reached about 43,9% from the global production. Input data for this software consists of load demand, cost of components, constraints, Resource data and system control [39].

HybSim is a hybrid energy simulation software was developed in 1987 by laboratory of sandia national [40], for sizing of isolated off grid hybrid energy system with combination of PV, DG and battery bank storage system and gave a good techno-economic analysis with prediction of operation and maintenance costs for component and high reliability. This tool requires detailed load demand, meteorological data, battery characteristics and economic details of each component [41].

TRNSYS (Transient Energy System Simulation Program) software was developed in 1975 by Wisconsin and Colorado university [42]. At starting used only for thermal systems simulation by the time became wide simulator for hybrid energy systems such as solar thermal and PV for facilities which require heating, ventilation and air conditioning (HVAC) system with energy saving strategy. This tool requires load demand and resource data as input and develops a detailed response for thermal and electrical energy system [43].

Dymola software was developed by the solar energy institute (ISE) in Germany, where it has an ability to size integrated energy system consists of solar PV panels, WT, DG, FC and batteries with LCC evaluation [44].

1.2.2. Sizing of Hybrid Energy System Using Traditional Methods

Traditional methods also called as deterministic sizing methods. The four most commonly used methods have been reported by sequence as following:

- **Analytical Method**

This method deals with the hybrid energy system as a number of numerical equations and considers sizing of the system as viability function, where in South Africa operated on sizing of PV panels and WTs for increasing efficiency of system with reasonable COE about 0,97 €/kWh with about 100 GWh every year [45], this approach has rapid execution but low flexibility in general use with optimization equations.

- **Iterative Approach**

This technique is an iterative algorithm that stops when the optimum design of proposed system is reached with desired objectives, where this method used to minimize COE and maximize reliability of integrated energy system consists of PV

panels, WTs and battery bank storage system in Brazil, where the LCC of this system reached about 25672\$ [46], this technique very easy in use but lacks for some important parameters such as hub height of WT, angle of blade rotation, tilt angle of solar PV panels, parameters of different radiation type.

- **Probabilistic Methods**

The probabilistic algorithm used to size the hybrid energy system taking into account the fluctuation in the wind speed and adjustments of the system component which effect on generated power from WTs. This method is simple in use but is not efficient to give optimal values, where it used to size energy system of solar PV panels /WT/biomass generator/ battery bank storage system but it maximized the storage capacity and rating of system component then increase the total system cost [47], this approach like probabilistic method easy in use but cannot provide a hybrid system's dynamic performance.

- **Artificial Intelligence Methods**

This an advanced method which used to control, configure and size each component of integrated energy system based on capacity of machine to carry out comparable tasks to those that make up the human mind [48]. There are several methods which simulate artificial algorithm such as multi-objective self-adaptive differential evolution algorithm (MOSADE) [49], mine blast algorithm (MBA) [50], preference inspired coevolutionary algorithm (PICEA) [51], Artificial bee swarm algorithm [52], artificial neural network (ANN) [53], fuzzy logic [54] and discrete harmony search (DHS) [55].

1.2.3. Sizing of Hybrid Energy System Using Metaheuristic Algorithms

In light of the previous review and study of different sizing methods we found that each method has no ability to achieve the best optimal solutions with the desired multi-objective function. So, an effective and widely applied techniques of metaheuristic techniques have been developed in the last decade [56]. These algorithms outperform all previous commercial software and traditional-deterministic methods in sizing of integrated RE systems. The most effective methodology which combines RE sources (solar PV panels, WTs, biomass generator, biogas generator, tidal...etc.) with traditional energy sources (DG) is called hybridization. We will review some artificial algorithms used in sizing of solar PV panels /WT /DG/battery bank energy system with different objective functions as summarized in Table 1 and illustrated as following:

In [57,58], a practical strategy called strength pareto evolutionary algorithm (SPEA) was used to optimize size of a solar PV panels /WT/DG hybrid energy system with minimization of total system cost and released amount of greenhouse gases, consequently two objective functions are used.

In [59-61], an efficient optimization technique called genetic algorithm (GA) has been developed to size and configure a solar PV panels /WT/battery hybrid energy system with multi-objective function such as maximizing reliability of the system under any uncertainty of wind speed and solar radiation, minimizing the LCC of the system and the LPSP.

In [62,63], an adaptive artificial method called particle swarm optimization (PSO), while it the most commonly used strategy for optimum sizing of hybrid energy system consists of PV/WT/DG/battery storage system with uncertainty consideration of natural resources. Also, in [64], PSO has been introduced to sizing a hybrid PV/WT/FC/electrolyzer/hydrogen tank /battery banks system with taking uncertainty of wind generation and reliability constraints of the system.

In [65], the simulated annealing algorithm (SAA) is optimization techniques has been applied to optimize size of integrated RE system of a PV/WT, where the algorithm operates on minimization of LCC of the system as an objective function.

In [66], a new algorithm called response surface methodology (RSM) has been applied in order to provide an optimum size of an integrated solar PV panels/WT/battery bank system with minimizing of LPSP and consumed amount of fossil fuel after that all results are compared with outcomes from previous simulated annealing algorithm.

In [67], depending on previous two adaptive optimization techniques (PSO and GA) any mathematical models of hybrid energy system can be introduced and then several objective optimizations were performed.

In [68], a featured comparison between results of the two effective algorithms (PSO and GA) where the used objective functions are maximizing reliability and minimizing the LCC of the system from the comparison, we found that the PSO approach presented its strength in terms of convergence, speed, and accuracy for handling the optimization issues.

In [69,70], a modified adaptive technique called multi-objective particle swarm optimization (MOPSO) has been implemented in order to minimize energy cost (COE), increase the system dependability and decrease outage of the feeding system for a hybrid PV/WT/FC/hydrogen storage system, where all results are compared with outcomes from particle swarm optimization method and it has proven its efficiency and ability to investigate.

In [71], a new effective combination of two optimization strategies; the first is sequential Monte Carlo simulation (SMCS) and the other is pattern search (PS), where this combination is used to optimize the sizing of hybrid energy system with reducing the system's LCC and fulfilling the system's reliability requirements. Additionally, a comparison with a hybrid GA-SMCS was conducted, and the results showed that the PS-SMCS performed better.

In [72], a modified meta-heuristic optimization method called cuckoo search algorithm (CS) has been developed to optimize size of isolated PV/WT/DG/battery energy system, where this method proved its strength in accurate results compared with genetic algorithm (GA) and particle swarm optimization (PSO).

In [73], a modern techniques called multi-objective self-adaptive differential evolution (MOSADE) algorithm designed to optimize size of a PV/WT/DG/battery hybrid energy system in city of Yanbu (KSA), where reduction of processing time is the multi-objective function.

In [74], an adaptive artificial method called artificial bee colony algorithm (ABC) has been developed to size and model a

on-grid solar PV panels /WT/battery integrated energy system with optimal cost of COE and highest reliability.

In [75], a modified effective technique called improved arithmetic optimization algorithm (IAOA) that created by modifying the original arithmetic optimization algorithm (AOA), while it has been used for giving the optimal size of a PV/WT/DG/battery also for PV/DG/battery hybrid energy system with minimizing the total system cost as an objective function.

Table 1: Comparison between metaheuristic algorithms for sizing of hybrid energy system components

Metaheuristic Algorithms	Applied Energy System	Objective Functions					DSM	Ref
		COE	GHGs	LPSP	Dummy Energy	Uncertainty		
SPEA	PV/WT/DG	✓	✓	--	--	--	--	(57,58)
GA	PV/WT/Bat	✓	--	✓	--	✓	--	(59,60)
PSO	PV/WT/DG/Bat & PV/WT/FC/Bat	✓	--	✓	--	✓	--	(62:64)
SSA	PV/ WT	✓	--	--	--	--	--	(65)
RSM	PV/WT/Bat	✓	✓	--	--	--	--	(66)
GA & PSO	PV/WT/DG/Bat	✓	--	✓	--	✓	--	(67,68)
MOPSO	PV/WT/FC/H ₂ storage tank	✓	--	✓	--	--	--	(69,70)
SMCS & PS	PV/WT/DG/Bat	✓	--	✓	--	--	--	(71)
CS	PV/WT/DG/Bat	✓	--	✓	--	✓	--	(72)
MOSADE	PV/WT/DG/Bat	✓	--	✓	--	--	--	(73)
ABC	PV/WT/Bat	✓	--	✓	--	--	--	(74)
IAOA	PV/WT/DG/Bat & PV/DG/Bat	✓	✓	--	--	--	--	(75)
WOA & MFO & WCA	PV/WT/DG/Bat	✓	--	✓	--	--	--	(76)

In [76], a newly created meta-heuristic optimization method known as whale optimization algorithm (WOA), water cycle algorithm (WCA) and moth-flame optimizer (MFO) are used strategy for optimizing size of integrated energy system consists of PV/WT/DG/battery storage system with reducing the system's LCC, fulfilling the reliability criteria in addition to efficiency of the system presented by LPSP.

1.3. Energy Saving and Reliability Concepts

Incoordination between load demand and available generation from different energy sources is the most issue which face the performance of microgrid where it increases COE due to huge expansion of the generation and distribution networks to satisfy amount of load demand at any time in addition to forcing most of energy sources to operate out of their rated capacity often at their maximum rating during peak load periods [77]. Therefore, balancing the load value with the available generated energy it might be beneficial to reduce these demands to avoid the need for more costly installations [78].

The load curves should be flexible as possible as it can for a number of reasons, lightening the strain on equipment of generated power consequently allow the microgrid's protection devices to operate as intended, in addition to minimizing costs of generated

energy and saving energy band for future load expansion. Accordingly, we will present and apply strategies of demand-side management (DSM). Reliability of any system is very important aspect, where a measure of system strength. It depends on nature of source with load at any internal and external faults which very important in determining the optimum size as following:

1.3.1. Demand Side Management Strategy

Desire for matching the load demand with available generation to overcome the peak load periods. DSM has several techniques, including “peak clipping, valley filling, load shifting, energy conservation, load building and flexible load shape” [79]. Which are illustrated in **Figure 3** and described as following [80]:

Peak clipping: This strategy is used when the capacity of the microgrid cannot satisfy the loads during the peak periods where this technique has been used to decrease load demand at peak times. Often, this is achieved by either forcing consumers to change their consumption patterns by raising the energy price (Electricity tariff) or by turning off particular appliances during peak hours.

Valley filling: This strategy is used to raise loads at off-peak times when generation exceeds loads in order to raise average energy consumption. In order to reduce the price of energy (electricity tariff), this strategy can be implemented by turning on low-importance loads and encouraging consumers to do activities like loading and charging during off-peak hours.

Load shifting: This strategy is used to shift low priority loads from peak to off-peak times without changing the pattern of energy consumption. Customers can store thermal heat during valley hours, for instance, and utilize it to keep the room warm all day. To prevent peak loading, it is also possible to increase the load factor of the load curve and get past the crucial peaks and valleys by running other household appliances like the dishwasher and washing machines at night. This can be achieved by raising the price of energy during peak hours and lowering it during off-peak.

Flexible load shape: This strategy sometimes called dynamic load management where the load is controlled according to the amount of generated energy that is available and it may be handled in exchange for the advantages. Using a dynamic electricity tariff to maintain price increases and decreases is one way to implement this technique.

Load conservation: This strategy sometimes called energy saving technique where is applied to use energy-efficient technologies to reduce the demand for energy additionally achieved by increasing the electricity bill or shutting down unnecessary loads, both of which lower load demand and change load shape.

Load building: This strategy is used to raise load during the load period because generation exceeds demand; load increases are necessary to keep the system stable, improve load-sharing, and boost grid responsiveness through energy storage systems. The energy price can be raised to achieve this.

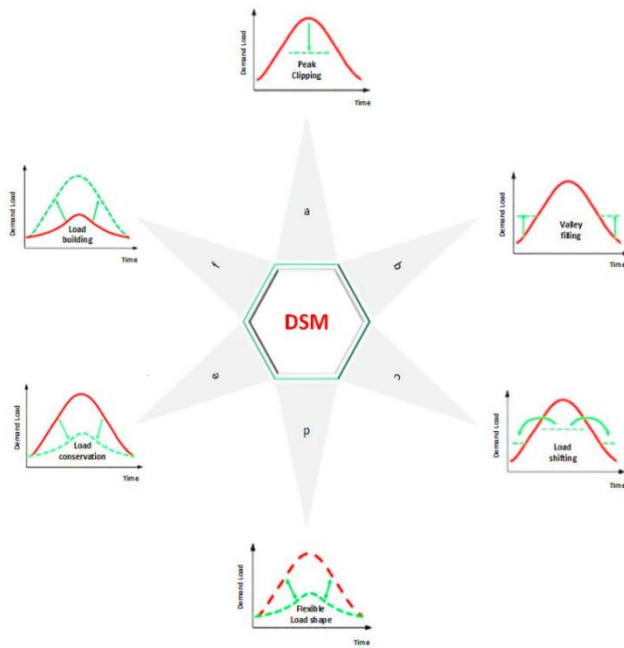


Figure 3: Demand-side management strategies

1.4. Contribution and Paper Organization

Starting with the requirement to harness RE sources to their fullest in order to diversify the production of power, this paper provide a cost-effective optimized design of an isolated RE system consists of integrated PV/WT/DG/battery bank based on high performance optimization techniques based SSA algorithm in comparison with some other meta-heuristic techniques. Depending on successful strategies like DSM, CC, and LF to reduce the amount of dummy energy and the LPSP, which limit the COE, while increasing the reliability and efficiency of the presented system. The following succinctly describes the primary contributions of this paper:

- System analysis has been introduced by high-efficient metaheuristic algorithms for tackling design problem of integrated RE system, which outperform all commercial software and traditional-deterministic methods. We have produced a detailed review and analysis along with a thorough comparison of various methods.
- Considering the multi-objective function that this study suggests in order to establish the optimum size of each component in a stand-alone hybrid PV/WT/DG/battery bank energy system through assessing the minimum COE, LPSP and amount of dummy energy at highest reliability and performance It resulted in considerable enhancements to the system's functionality.
- Providing a detailed methodology to achieve the HRES's maximum power output and the lowest cost of the energy it supplies.
- Utilizing efficient techniques like DSM, CC, and LF with different techniques such as load shifting, peak clipping, energy conservation, valley filling, flexible load shape and load building, which have significant effect on satisfying the

load demand and decreasing the system's component sizes, and lastly, the life cycle cost.

- Supplying the solar radiation and wind speed data for city of New Minia located in Egypt, they are obtained from two sources:
 - The National Space and Aeronautics Authority (NASA) data.
 - The meteorological data' long-term average over a 20-year period of observation.
- To the best of the author' knowledge, generally speaking, in order to develop this planned remote area, this is the first attempt to optimize the system components based on meteorological data and real-time information of New Minia city, situated in Egypt.

2. Development of an IHRES

The following stages explain a systematic approach that is necessary to implement an IHRES for isolated communities:

2.1. Identification of Study Area

The New Minia city of Minia governorate in Egypt is considered as a study area, where the city is located on the right bank of the Nile across from Old Minia. **Figure 4** displays its location on a map. It is located at a height of 123 meters above mean sea level, in latitude 28.0986° N and longitude 30.8327° E.

2.2. Visualization of Electrical Demand

This study based on supply electricity to utilities and infrastructure sector in the New Minia city which can be summarized in residential, commercial and industrial sector with 6 districts, clubs' area, build your own house areas, roads, communications and extension area networks are being implemented. In addition to a wells plant of drinking water, sanitation plant of 4 pumping and cultivation of green areas and forestation. **Figure 5** shows the hourly load power used for the system in this work, which has an average load demand of around $2.25 \cdot 10^4$ kW, a peak load of $4.2 \cdot 10^4$ kW, and a minimum load of $0.7 \cdot 10^4$ kW.

2.3. Assessment of Natural Resources

Meteorological data develops the average annual wind speed at the New Minia city, which is approximately 5.19 m/s at 10m height (Anemometer suspension level) as shown in Figure 6. Furthermore, meteorological data represents the annual average curve of solar energy for the selected site, where Figure 7 illustrates the average 24 years (1994-2018) that the study took into account for the simulation, which around 6.05 kWh/m²/day. The annual average curve of ambient temperature from meteorological data is shown in Figure 8. In the simulation, the study took into account a 24-year average (1994-2018) with an average temperature of 25.58°C (78.04°F).

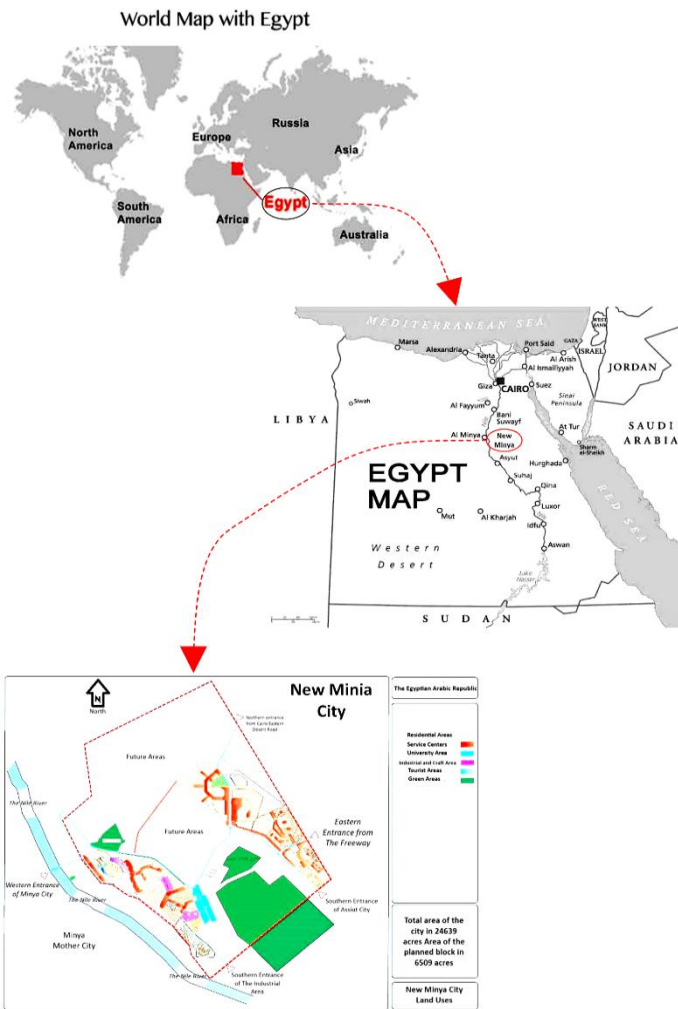


Figure 4: The location of the studied village, namely The New Minia city located in the middle-east of Egypt

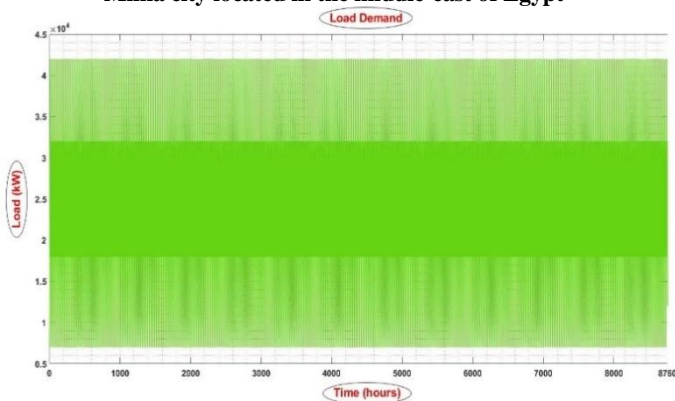


Figure 5: Hourly load power for the New Minia city

After looking at the meteorological data for the studied site, including the average annual wind speed, solar energy, and ambient temperature, we came to the conclusion that this location is ideal for utilizing some RE sources. Such as solar PV panels and wind farms, which are thought to be sustainable and likely to be financially competitive given that their costs are significantly lower in the medium range than those of traditional energy sources.

Furthermore, the utilization of sustainable energies confers significant benefits to isolated areas, especially for the availability of energy resources to those who are currently without them.

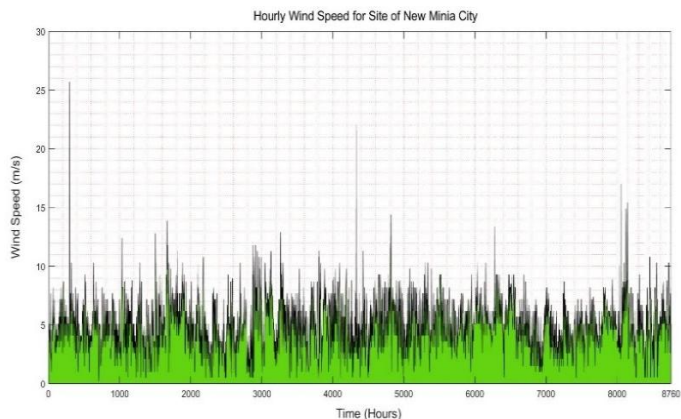


Figure 6: The average annual wind speed of the New Minia city

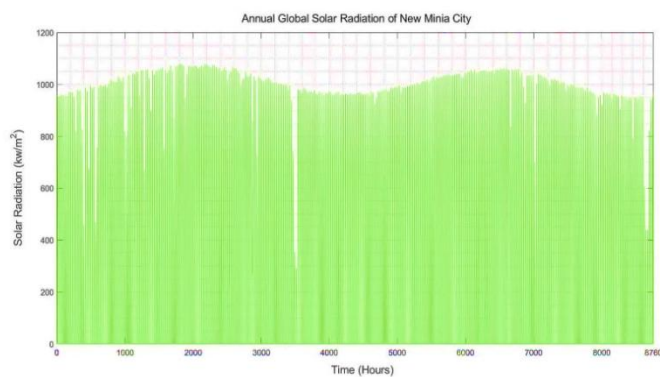


Figure 7: The average annual solar energy of New Minia city

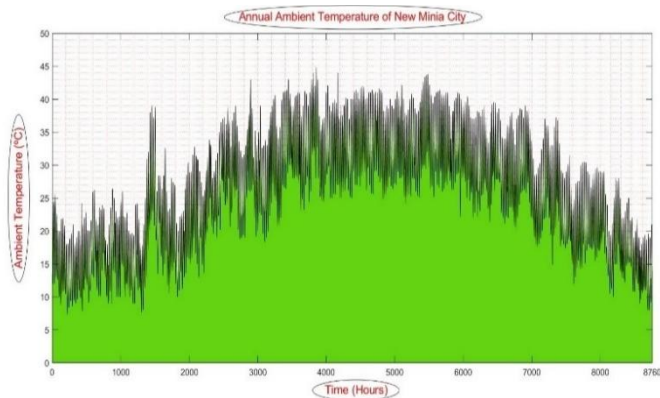


Figure 8: The hourly ambient temperature for the site of the New Minia

For economic reasons, sustainable energy has been completely ignored up to this moment. However, the trend in recent years has been toward sustainable energy instead than conventional energy.

3. Mathematical Modelling of the IHRES Components

A proper mathematical modeling of the component parts is required before determining the ideal size for the IHRES. In addition to solar and wind energy, the research suggests an IHRES-

model that includes a DG as a backup power and a battery bank storage system. The shortage of electricity in the city of New Minia may be economically resolved with construction of an integrated PV/WT/DG/battery bank hybrid RE system. Seven primary components make up the proposed hybrid microgrid system under study, as represented in **Figure 9**. These include solar PV modules, WT's, a DG, a battery bank storage system, a bi-directional power converter, a dump load, and a service load.

3.1. Wind Energy System Model

Wind resources and WT's capacity to generate energy at a certain location are affected by wind speed at hub height, WT speed characteristics, and land surface type. Given the wind speed observed at the anemometer height, where the wind speed at the required hub height may be expressed as follows [87]:

$$u(h) = u(h_a) \left(\frac{h}{h_a}\right)^\alpha \quad (1)$$

Where, $u(h)$ is the wind speed at hub height in (m/s), $u(h_a)$ is the measured wind speed in (m/s), and α is roughness factor which varies periodically and from site to site. As per the guidelines provided by IEC standards [88], according to calculations, the coefficient of friction is 0.20 under normal wind conditions and 0.11 in strong wind conditions and has been taken by (1/7) in this paper.

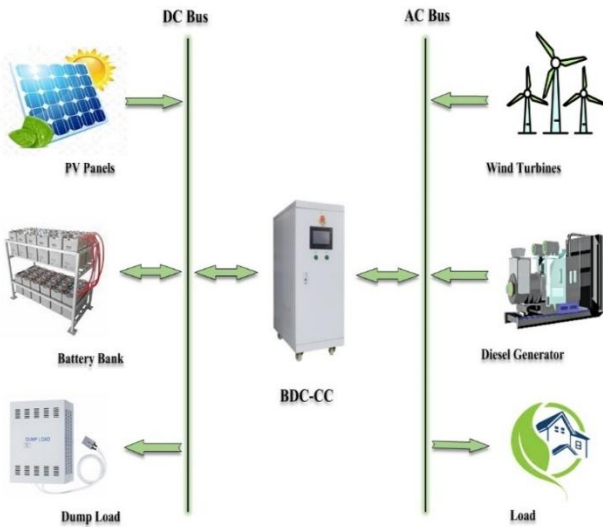


Figure 9: The configuration of the IHRES

The basic formula that controls the WT's mechanical output power estimated as follows:

$$P_{mech} = \frac{1}{2} \rho A C_p u^3 \quad (2)$$

Where, A is the rotor blade swept area (m^2), u is the wind speed (m/s), C_p is the WT's power coefficient, and ρ is the air density (kg/m^3). The power coefficient C_p sometimes called Betz's coefficient, it is the function of the rotor tip-speed to wind speed ratio (λ) as follows, with a theoretical maximum value of 0.593 [89]:

$$\lambda = \frac{\omega R}{u} \quad (3)$$

Where, R is the WT radius (meters), and ω is the turbine's angular velocity (rad/sec). The features of a WT's power production at a constant wind speed are displayed in **Figure 10**.

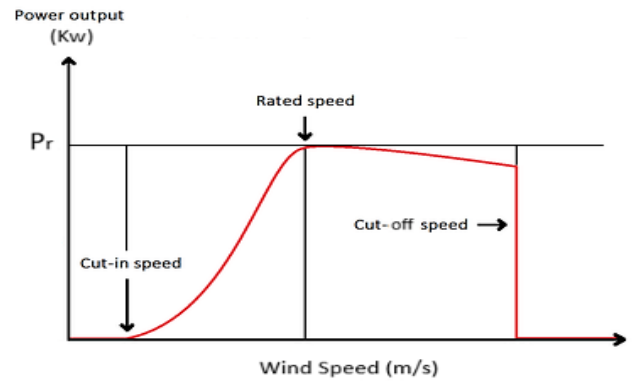


Figure 10: Wind turbine power characteristics

The wind speed at which a turbine initially turns and starts to generate energy is referred to as the "cut-in speed." Cut-off speed is the high wind speed that puts significant stresses on the turbine construction and raises the risk of rotor damage. The braking mechanism is utilized to stop the rotor in order to avoid damage. The rated power output of an electrical generator is the wind speed that falls between the cut-in and cut-off speeds, at which point the generator's maximum power output is achieved.

Based on the normal power curve parameters of the WT, the estimated power delivered by the turbine P_{WT} may be described as the following [90,91]:

$$P_{WT} = \begin{cases} 0 & u(t) < u_{cut-in} \\ \frac{\eta_{WT} * P_{R_{WT}} * (u^2(t) - u^2_{cut-in})}{u^2_{rated} - u^2_{cut-in}} & u_{cut-in} \leq u(t) \leq u_{rated} \\ \eta_{WT} * P_{R_{WT}} & u_{rated} < u(t) \leq u_{cut-off} \\ 0 & u(t) > u_{cut-off} \end{cases} \quad (4)$$

Where, N_{WT} is the number of used WT's, u_{cut-in} is the cut-in wind speed, u_{rated} is the rated wind speed and $u_{cut-off}$ is the cut-off wind speed; and $P_{R_{WT}}$ is the rated WT output power.

The wind energy capacity at any particular location may be estimated statistically by analyzing the wind speed data using the Weibull distribution. There are several methods for computing the Weibull parameters k and c . The probability density function for wind speed (u) in a two-parameter distribution as following [92]:

$$f(u) = \frac{k}{c} * \left(\frac{u}{c}\right)^{k-1} * \exp\left[-\left(\frac{u}{c}\right)^k\right] \quad \text{where, } (k > 0, u > 0, c > 0) \quad (6)$$

Where, k is the shape parameter and c are the scale parameter, and the following formula may be used to get the cumulative distribution function (u):

$$F(u) = 1 - \exp\left[-\left(\frac{u}{c}\right)^k\right] \quad (7)$$

The following formulas are the Weibull parameters' final results:

$$k = a \quad \text{and} \quad c = \left(-\frac{b}{k}\right) \quad (8)$$

Where, parameters a and b can be estimated respectively, as the following:

$$a = \frac{(\sum_{i=1}^w (x_i - \bar{x}) * \sum_{i=1}^w (y_i - \bar{y}))}{(\sum_{i=1}^w (x_i - \bar{x})^2)} \quad (9)$$

$$b = \bar{y}_i - ax_i = \left(\frac{1}{w} \sum_{i=1}^w y_i - \frac{a}{w} \sum_{i=1}^w x_i\right) \quad (10)$$

$$y_i = \ln\left(-\ln(1 - F(u_i))\right) \quad \text{and} \quad x_i = \ln(u_i) \quad (11)$$

Where, w is the number of non-zero wind speeds, u_i is the wind speed (m/s) at time step i, and x_i and y_i 's average values are \bar{x} and \bar{y} , respectively.

This formula that may be used to find the capacity factor at C_F a certain location as the following:

$$C_F = \frac{\exp\left[-\left(\frac{u_{cut-in}}{c}\right)^k\right] - \exp\left[-\left(\frac{u_{rated}}{c}\right)^k\right]}{\left(\frac{u_{rated}}{c}\right)^k - \left(\frac{u_{cut-in}}{c}\right)^k} - \exp\left[-\left(\frac{u_{cut-off}}{c}\right)^k\right] \quad (12)$$

The energy produced from WT panels (E_{WT}) is calculated as the following:

$$E_{WT}(t) = N_{WT} * C_F * P_{WT}(t) * \Delta t \quad (13)$$

Where, Δt represents the time interval and is equivalent to one hour.

3.2. Solar Energy System Model

In the literature, several models for calculating PV output power have been put forth. The output power of a PV panel has been determined in this research using a simplified model. $P_{PV}(t)$ based on the research area's hourly solar radiation $G(t)$ and hourly ambient temperature T_{amb} [92] may be estimated as the following:

$$P_{PV}(t) = PV_{panel_rating} * \left(\frac{G(t)}{G_{ref}}\right) * [1 + K_T * (T_C - T_{ref})] \quad (14)$$

Where, PV_{panel_rating} is the PV panel rated power, G_{ref} is solar radiation used as the reference condition, with a value of 1000 (W/m^2), K_T is the temperature coefficient of maximum power, with a value of 3.7×10^{-3} ($1/^\circ C$), T_C is the cell average annual temperature ($^\circ C$) and T_{ref} is the temperature of the PV cell in standard test conditions (STC), with a value of $25^\circ C$.

The cell averages annual temperature T_C may be calculated as the following:

$$T_C(t) = T_{amb} + \left[\left(\frac{NOCT-20}{0.8}\right) * \left(\frac{G(t)}{G_{ref}}\right)\right] \quad (15)$$

Where, T_{amb} is the ambient temperature ($^\circ C$), and $NOCT$ is the normal cell temperature during operation. with a value of $45^\circ C$ for the selected PV module under study.

The energy generated $E_{PV}(t)$ from number of PV panels N_{PV} is calculated as the following:

$$E_{PV}(t) = N_{PV} * P_{PV}(t) * \Delta t \quad (16)$$

where, Δt represents the time interval and is equivalent to one hour.

3.3. Battery Storage System Model

In most cases, the battery bank supplies the system during periods of high load demand or when RE supplies are unavailable. We'll store any excess energy generated by the RE resources in the battery bank. The energy stored in the battery bank at each given hour " t + 1 " is represented by the following formulae [93, 94]:

$$E_{Bat}(t + 1) = (1 - \sigma) * E_{Bat}(t) + \left(P_{Gen}(t) - \frac{P_{Load}(t)}{\eta_{Conv}}\right) * \Delta t * \eta_{CC} * \eta_{BC} \quad (17)$$

During the discharge process, the electrical power produced by the RE resources is insufficient to meet the load requirement. As a result, the battery bank is capable of providing the necessary shortfall load, which is as the following:

$$E_{Bat}(t + 1) = (1 - \sigma) * E_{Bat}(t) - \left(\frac{P_{Load}(t)}{\eta_{Conv}} - P_{Gen}(t)\right) / \eta_{BD} * \Delta t \quad (18)$$

Where, $P_{Load}(t)$ is the load power demand, $P_{Gen}(t)$ is the total electrical power generated, and σ is the rate of self-discharge every hour. For most batteries, the manufacturer's datasheet recommends a value of 0.2% per day [59]. Battery charging and discharging efficiencies are represented by η_{BC} and η_{BD} , which are estimated to be 90% and 85%, respectively, [95]. Bi-directional converter efficiency is represented by η_{Conv} , which is estimated to be 95% [96].

The amount of power produced by the RE resources, $P_{Gen}(t)$ is calculated as the following:

$$P_{Gen}(t) = [P_{PV}(t) + P_{WT}(t)] * \eta_{Conv} \quad (19)$$

3.4. Diesel Generator Backup System Model

Internal Combustion DGs are useful in isolated grid areas because they supply electricity when RE sources are interrupted by protracted cloud cover or wet seasons, or in the event that batteries cannot supply the required load. Based on the necessary load demand, the DG hourly fuel consumption (F_{DG}) may be computed using the following linear rule [93]:

$$F_{DG}(t) = [a_{DG} * P_{DG_Gen}(t) + b_{DG} * P_{DG_rating}] (l/h) \quad (20)$$

Where, the fuel consumption curve for DG, the coefficients a_{DG} and b_{DG} have the values $a_{DG} = 0.246$ (l/kwh) and $b_{DG} = 0.08145$ (l/kwh), respectively [58,97]. The DG's rated power and hourly generated power are indicated by P_{DG_rating} and $P_{DG_Gen}(t)$, respectively.

The following formula is used to get the DG annual fuel consumption (AFC):

$$AFC = \sum_{t=1}^{8760} F_{DG}(t) \quad (21)$$

3.4.1. CO₂ Emissions

DG's hourly fuel usage and CO_2 emissions may be estimated as follows [98]:

$$CO_2(t) = SE_{CO_2}(kg/l) * F_{DG}(t) (l/h) \quad (22)$$

where, the specific CO_2 emissions per liter of diesel are represented by SE_{CO_2} , and its value is 2.7 kg/l .

The following is an estimation of the DG's yearly CO_2 emissions:

$$Annual_{CO_2_Emissions} = \sum_{t=1}^{8760} CO_2(t) \quad (23)$$

3.5. Bidirectional or Dual Converter with a Charge Controller (BDC-CC) Model

Generally speaking, electrical energy is converted by the BDC-CC into rectifier and inverter operating modes. In the inverter mode, it converts Direct Current (DC) to Alternate Current (AC), and in the rectifier mode, it converts AC to DC. To make sure the battery bank is neither over-charged nor over-discharged, the charge controller is helpful. The following formulas is used to compute the BDC-CC power rating (P_{BDC-CC}) depending in mode of operation [78]:

- Wind turbine produces more power than demand load $P_{WT}(t) > P_{Load}(t)$ or in another form power that generated from both WTs and PV panels very larger than demand load $P_{WT}(t) + P_{PV}(t) \gg P_{Load}(t)$ where, the converter starts to charge battery (if $E_{Bat}(t) < E_{Bat_max}$). So, sizing of the BDC-CC may be estimated as the following:

$$P_{BDC-CC}(t) = [P_{WT}(t) - P_{Load}(t)] * \eta_{Conv} \quad (24)$$

- WT produces less power than demand load $P_{WT}(t) < P_{Load}(t)$ or $P_{WT}(t) + P_{PV}(t) > P_{Load}(t)$ and (if $E_{Bat}(t) < E_{Bat_max}$) battery starts to charge, but if it is charged all surplus power will flow to the dump load. So, sizing of the BDC-CC may be estimated as the following:

$$P_{BDC-CC}(t) = [P_{PV}(t) - P_{Load}(t)] * \eta_{Conv} \quad (25)$$

- WT and PV panels produce less power than demand load $P_{WT}(t) + P_{PV}(t) < P_{Load}(t)$, where deficit in power of demand load is supplied from battery bank but (if $E_{Bat}(t) > E_{Bat_min}$), so discharged power from battery starts flows through the converter towards the load. So, sizing of the BDC-CC may be estimated as the following:

$$P_{BDC-CC}(t) = [P_{PV}(t) + P_{WT}(t)] * \eta_{Conv} \quad (26)$$

The previous formulas may be used to calculate the necessary PWM converter rated power based on the simulation's findings [99].

3.6. System Reliability Model

Reliability is the ability of the power system to deliver energy for a predetermined period of time under specific conditions. In this study, the power dependability of the IHRES is assessed using the $LPSP$, which is calculated by adding the hours of a power outage to the sum of hourly energy demands. Calculating the LPS at any hour "t" is done using the formula below [100]:

$$LPS(t) = \frac{P_{Load}(t)}{\eta_{Conv}} - P_{Gen}(t) - [(1 - \sigma) * E_{Bat}(t+1) - E_{Bat}(t)] * \eta_{BD} \quad (27)$$

The $LPSP$ is calculated as follows [134]:

$$LPSP = \frac{\sum_{t=1}^{8760} LPS(t)}{\sum_{t=1}^{8760} P_{Load}(t)} \quad (28)$$

3.7. Economic Analysis of The Off-Grid IHRES

The IHRES's economic sustainability has been evaluated using a variety of methods, including Net Present Cost, Annual Levelized Cost, LCC , and Payback Period. Since the LCC technique offers an exact representation of project costs during the project's life cycle, it is often used in these scenarios for economic analysis. Using the following formula [100], the LCC of the IHRES is determined in this study by adding all costs associated with system component replacement, erection, initial capital, $O\&M$, and fuel. COE is one of the most prominent and extensively used indicators in IHRES economic approach, and may be computed as follows [75]:

$$COE = \frac{LCC * CRF(i, T)}{\sum_{t=1}^{8760} P_{Load}(t)} \quad (32)$$

where, T is the project lifetime in years. In this study is chosen as 25 years. i is the real net interest rate, and CRF is the factor for capital recovery which can be computed by applying the following formula [59]

$$CRF(i, T) = \frac{i * (1+i)^T}{(1+i)^T - 1} \quad (33)$$

The discount rate be computed by applying the following formula [79]:

$$y = \frac{i_{nom} - f}{1 + f} \quad (34)$$

where, the yearly nominal interest rate is denoted by i_{nom} . About 8.25% is found in this research [101]. A yearly inflation rate is denoted by f . This study's estimate is 4.9% [102].

The life cycle cost (C_{Life_Cycle}) of the overall project can be estimated by using the following formula:

$$LCC = C_{Initial_Capital} + C_{O\&M} + C_{Rep} + C_{Fuel} - V_{Scarp} \quad (35)$$

where, $C_{Initial_Capital}$ is the initial capital costs, $C_{O\&M}$ is the operation and maintenance costs, C_{Rep} is the replacement costs, C_{Fuel} is the fuel costs, $C_{Erection}$ is the erection costs and V_{Scarp} is the scrap present value of each component of the IHRES.

Costs of installation, civil works, electrical testing, and commissioning are all included in $C_{Initial_Capital}$. This paper assumes that the costs of installation and civil works account for 20% of WT system costs and 40% of solar system costs, respectively [99]. $C_{Initial_Capital}$ may be estimated as the following:

$$C_{Initial_Capital} = C_{WT} * P_{RWT} * N_{WT} + C_{PV} * P_{V_{panel_rating}} * N_{PV} + C_{Bat} * S_{Bat_rating} * N_{Bat} + C_{DG} * P_{DG_rating} * N_{DG} + C_{BDC-CC} * P_{BDC-CC} \quad (36)$$

where, C_{WT} is the cost of WT including civil works (\$/kw), P_{RWT} is the rated WT output power, N_{WT} is the number of used WTs, C_{PV} is the cost of PV panels including civil works (\$/kw), $P_{V_{panel_rating}}$ is the PV panel rated power, N_{PV} is the number of PV panels, C_{Bat} is the COE storage batteries (\$/kw), S_{Bat_rating} is the rating of battery bank, N_{Bat} is the number of battery cells, C_{DG}

is the cost of DG system, $P_{DG_{rating}}$ is the DG system's rated power and N_{DG} is the number of DGs.

The estimated $C_{O\&M}$ values are compiled in this paper after a thorough analysis of several research [102-105]. This may be computed using the following formula [106]:

$$C_{O\&M} = \sum_{j=1}^T C_{O\&M}(1) * \left(\frac{1}{(1+i)^j}\right) \quad (37)$$

where, $C_{O\&M}(1)$ is the project's first-year operating and maintenance costs. There is another formula which can be expressed as:

$$C_{O\&M} = C_{O\&M_WT} * T_{WT} + C_{O\&M_PV} * T_{PV} + C_{O\&M_Bat} * T_{Bat} + C_{O\&M_DG} * T_{DG} + C_{O\&M_BDC-CC} * T_{BDC-CC} \quad (38)$$

where, $C_{O\&M_WT}$, $C_{O\&M_PV}$, $C_{O\&M_Bat}$, $C_{O\&M_DG}$ and $C_{O\&M_BDC-CC}$ are the cost of maintenance and operation for each component of time for WT, PV panels, battery storage systems, DGs, and bidirectional converters. While, T_{WT} , T_{PV} , T_{Bat} , T_{DG} and T_{BDC-CC} are the operating time of WT, PV, battery storage banks, DG and bidirectional converter, respectively.

The following formula may be used to determine the present value of the replacement cost of the hybrid system components C_{Rep} over the period of the system's lifespan:

$$C_{Rep} = \sum_{j=1}^{N_{Rep}} [K_{Rep} * C_u * \left(\frac{1}{(1+i)}\right)^{\left(T * \frac{j}{N_{Rep}+1}\right)}] \quad (39)$$

Where, K_{Rep} , C_u and N_{Rep} are the replacement components capacity (kw for WT system, PV panels, DG and bidirectional converters and kwh for batteries), the costs of the replacement components (\$/kw for WT system, PV panels, DG and bidirectional converters, and \$/kWh for batteries) and the number of replacements during the lifespan of the project T, respectively.

The fuel cost of C_{Fuel} , can be calculated from the following formula:

$$C_{Fuel} = \left(\sum_{t=1}^{8760} F_{DG}(t)\right) * P_{Fuel} \quad (40)$$

where, $\sum_{t=1}^{8760} F_{DG}(t)$ is the DG annual fuel consumption (l), P_{Fuel} is the price of fuel per liter, where (The price of fuel is taken in this paper 0.8 \$/l).

This following formula may be used to determine the V_{Scarp} :

$$V_{Scarp} = \sum_{j=1}^{N_{Rep}+1} [SV \left(\frac{1}{(1+i)}\right)^{\left(T * \frac{j}{N_{Rep}+1}\right)}] \quad (42)$$

where, SV is the scrap value of the project components.

4. Objective Function

The objective function, which is the minimal value of the system energy cost and determined by using the formula (34). Where all these cost types are a function of some important-selected variables, which involved in the optimization such as N_{WT} , N_{PV} , N_{Bat} and DG rating considering the below system constraints. This is clear that the system model is nonlinear depending on previous techno-economic mathematical model, which will be analyzed by using effective metaheuristic algorithm. The following equation expresses the objective function as shown:

$$\min COE(N_{WT}, N_{PV}, N_{Bat}) = \sum_{C=WT, PV, BAT, DG, BDC-CC}^{\min} (LCC)_c \quad (43)$$

4.1. Upper and Lower Bounds

In this study we assumed that the PV array and WTs operate as the microgrid's primary energy sources; hence, in the event of an energy excess, the battery begins to charge, but if there is a deficit energy the battery discharge to meet load (if it is charged). Hence, the wind, solar PV energy resources and the battery bank is subject to the following constraints:

$$N_{WT_min} \leq N_{WT} \leq N_{WT_max} \quad (44)$$

$$N_{PV_min} \leq N_{PV} \leq N_{PV_max} \quad (45)$$

$$N_{Bat_min} \leq N_{Bat} \leq N_{Bat_max} \quad (46)$$

where, N_{WT} are the number of WTs, N_{PV} are the number of PV panels and N_{Bat} are the number of battery cells.

4.2. Battery Bank Storage System Limits

The following limits [93], determines the amount of energy that is stored in the battery bank at any particular time "t":

$$E_{Bat_min} \leq E_{Bat}(t) \leq E_{Bat_max} \quad (47)$$

Where, E_{Bat_max} and E_{Bat_min} are the maximum and minimum energy storage levels of the battery bank, respectively which may be calculated as the following:

$$E_{Bat_max} = \left(\frac{N_{Bat} * V_{Bat} * K_{Bat}}{1000}\right) * SOC_{Bat_max} \quad (48)$$

$$E_{Bat_min} = \left(\frac{N_{Bat} * V_{Bat} * K_{Bat}}{1000}\right) * SOC_{Bat_min} \quad (49)$$

where, V_{Bat} and K_{Bat} are the battery's voltage and rated capacity (Ah), where SOC_{Bat_min} and SOC_{Bat_max} are the battery's lowest and greatest states of charge, which may be calculated as the following:

$$SOC_{Bat_min} = 1 - DOD \quad (50)$$

$$SOC_{Bat_max} = SOC_{Bat_min} - DOD \quad (51)$$

where, DOD is the depth of discharge of the battery. Figure 11 shows the normal relationship between lead-acid battery life cycle and DOD.

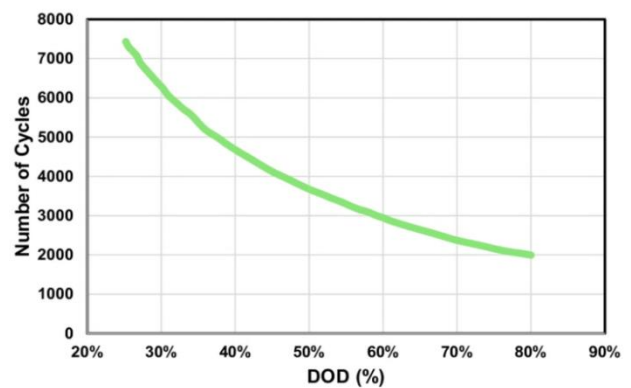


Figure 11: The typical lifecycle of RS lead acid-SSIG batteries versus DOD

4.3. Diesel Generator Operating Limits

The DG operates significantly more efficiently at greater loads. Therefore, 25% (taken into calculations in these paper) of the DG's rated capacity is the maximum load for it to operate. As a result, the DG will operate in operational mode after it complies with the following restrictions [31]:

$$\frac{P_{Load}(t)}{\eta_{Conv}} \leq 25\% \text{ of } P_{DG_rating} * \Delta t \quad (52)$$

where, $P_{Load}(t)$ is the demand load at every hour, η_{Conv} is the converter's efficiency, P_{DG_rating} is the DG's rated power, and Δt is the simulation's time duration.

4.4. Loss of Power Supply and Dump Energy Limits

The LPSP and dump energy (E_{Dump}) are two important indices which indicate the system reliability. The optimization approach has been developed to trace the LPSP and dump load values to fulfill the specific limits to achieve the lowest LEC. In this study, the permitted limit for LPSP and the permitted limit for dump energy is considered to be as follows:

$$LPSP \leq 5\% \text{ of } ADL \quad (53)$$

$$E_{Dump} \leq 2\% \text{ of } ADL \quad (54)$$

where, ADL is the total annual demand load which can be calculated as the following:

$$ADL = \sum_{t=1}^{8760} P_{Load}(t) \quad (55)$$

5. Energy Management Strategy

Energy management is thought to be an essential step in the IHRES sizing and optimization process. A suggested energy management method for the PV/WTs/DG/battery banks IHRES is presented in this paper. This algorithm's primary goal is to determine the ideal IHRES component size in order to satisfy load demand while staying within LPSP limitations and to dump energy (E_{Dump}) in order to minimize LEC. The suggested approach is reliant on calculating the IHRES's energy balance every hour of the year, where Figure 13 and Figure 14 show flowcharts of the EMS for the operating modes.

5.1. Methodology

The design of the IHRES requires a robust energy management strategy (EMS). The efficient distribution of power among the system's components is the main goal of the EMS. As a result of the DG using less fuel, more RE resources are being used. Significant cost and energy savings are achieved as a result of the EMS's increased system efficiency and reliability. Rule-based algorithms with "else," "elseif," "for" loop, and "if" conditions have been used to construct the suggested EMS. It simulates the input parameters, including load demand, wind speed, ambient temperature, solar irradiation, and techno-economic values of the components, for 8760 hours, or one year, in the MATLAB® environment. The recommended EMS for the IHRES by the LF and CC techniques is explained as follows:

• Load Following Strategy

The primary benefit of the LF approach is that it may be used when energy needs are greater than what batteries and RE sources can supply, the DG can meet the shortfall load requirement. The main issue is that it doesn't charge the batteries it just meets the shortfall load need. The following modes describe how the LF strategy functions overall [107]:

• Cycle Charging Strategy

The difference between the CC strategy and other strategies is that the DG will activate to meet the need for the shortfall load while maintaining the battery bank's energy reserves constant during the charging process. The following modes provide an overview of the CC strategy's general operation [29]:

Now, the 'for' loop will begin for 8760 hours of simulation.

for t=1:1:8760

$$P_{net}(t) = [P_{WT}(t) + P_{PV}(t) * \eta_{Conv}] - P_{Load}(t)$$

if $P_{net}(t) = 0$

Mode 1: In this mode of operation, the battery bank's energy level at time 't+1' is equal to the energy level of the preceding hour, and the system's total net power delivered is equal to 0. Whereas the switches S4, S5, and S5 are in the open position, the switches S1, S3, and S2 are closed. This mode of operation is illustrated clearly in Figure 12(a). There won't be a power outage and the anticipated load demand will be satisfied, which may be represented mathematically as follows:

$$P_{Bat_charging}(t) = 0$$

$$P_{Bat_Discharging}(t) = 0$$

$$E_{Bat}(t+1) = E_{Bat}(t)$$

$$LPS(t) = 0$$

$$P_{Dump}(t) = 0$$

elseif $[P_{WT}(t) + P_{PV}(t) * \eta_{Conv}] > P_{Load}(t)$

$$P_{Bat_charging}(t) = [(P_{WT}(t) - P_{Load}(t)) * \eta_{Conv} + P_{PV}(t)]$$

if $E_{Bat}(t) < E_{Bat_max} - E_{Bat}(t)$

Mode 2: In this mode of operation, the RE resources initially satisfy the load demand before storing the generated excess energy in the battery bank. This is only applicable if the energy levels inside the battery bank fall within the min-max range, that is, ($E_{Bat_min} \leq E_{Bat}(t) \leq E_{Bat_max}$). While the switches S4 and S5 are in the open position and the switches

S1, S2, and S3 are closed. This mode of operation is illustrated visually in Figure 12(b). There won't be a power outage and the anticipated load demand will be satisfied, which may be represented mathematically as follows:

$$E_{Bat}(t+1) = (1 - \sigma) * E_{Bat}(t) + P_{Bat_Charging}(t) * \eta_{BC}$$

$$LPS(t) = 0$$

$$P_{Dump}(t) = 0$$

else

Mode 3: In this mode of operation, the energy from the RE resources first meets the load requirement. If the battery bank's energy level reaches its maximum limit (that is, if $(E_{Bat}(t) = E_{Bat_max})$, then the dump load is operated using the extra energy. In this mode of operation, S2 and S4 switches are in the open position, while S1, S3, and S5 switches are closed, as seen in Figure 12(c). There won't be a power outage and the anticipated load demand will be satisfied, which may be represented mathematically as follows:

$$E_{Bat}(t+1) = E_{Bat_max}$$

$$LPS(t) = 0$$

$$P_{Dump}(t) = P_{Bat_Charging}(t) - [E_{Bat_max} - E_{Bat}(t)]$$

end

elseif $[P_{WT}(t) + P_{PV}(t) * \eta_{Conv}] < P_{Load}(t)$ and $E_{Bat}(t) \geq E_{Bat_max}$

Mode 4: In this mode of operation, the battery bank will supply the shortfall load need since the energy required to operate the RE resources is less than what is needed. ($E_{Bat}(t) \geq E_{Bat_max}$). S1, S2, and S3 switches are in the closed position, while S4 and S5 switches are in the open position, as shown in Figure 12(d). during this mode of operation. The anticipated load demand will be satisfied, there won't be a power outage, and they may be written mathematically as follows:

$$P_{Bat_Discharging}(t) = P_{Load}(t) - [P_{WT}(t) + P_{PV}(t) * \eta_{Conv}]$$

$$E_{Bat}(t+1) = (1 - \sigma) * E_{Bat}(t) - (P_{Bat_Discharging}(t) / \eta_{BD})$$

$$LPS(t) = 0$$

$$P_{Dump}(t) = 0$$

if

$$\frac{P_{Load}(t)}{\eta_{Conv}} \leq 25\% \text{ of } P_{DG_rating} \quad \text{and} \quad E_{Bat}(t) \leq E_{Bat_min}$$

Mode 5: When there is not enough energy to match the load demand from the battery bank and RE resources. The DG will thereafter be operational to meet the shortfall load requirement if $(E_{Bat}(t) \leq E_{Bat_min})$. As soon as the RE resources start to generate enough electricity to fulfill the demands of the entire load, the DG stops. S1, S3, and S4 switches are in the closed position during this mode of operation, whilst S2 and S5 switches are in the open position, as illustrated in Figure 12(e). the battery bank still as the previous state. It may be mathematically written as follows: The anticipated load demand will be satisfied, and which are mathematically expressed as follows:

$$P_{DG_Gen}(t) = P_{Load}(t) - [P_{WT}(t) + P_{PV}(t) * \eta_{Conv}]$$

$$E_{Bat}(t+1) = (1 - \sigma) * E_{Bat}(t)$$

$$LPS(t) = 0$$

$$P_{Dump}(t) = 0$$

else

Mode 6: In this mode of operation, there will be a power outage at time 't' because the battery bank's energy level is below the recommended minimum level and the energy supplied by the RE resources is less than the necessary load demand, i.e. $E_{Bat}(t) = E_{Bat_min}$, but the DG will operate at its maximum capacity as illustrated in Figure 12(f). This can be expressed mathematically as follows:

$$P_{DG_Gen}(t) = P_{DG_max}$$

$$E_{Bat}(t+1) = E_{Bat_min}$$

$$LPS(t) = P_{Load}(t) - [P_{WT}(t) + P_{PV}(t) * \eta_{Conv}] - P_{DG_max}$$

$$P_{Dump}(t) = 0$$

end

end

end

The total dump energy which extracted from the system can be calculated as the following:

$$E_{Dump} = \sum_{t=1}^{8760} P_{Dump}(t) \quad (56)$$

The LPSP which expressed in deficit energy in the system can be calculated as the following:

$$LPS_{Total} = \sum_{t=1}^{8760} LPS(t) \quad (57)$$

The total energy which consumed from the DG can be calculated as the following:

$$E_{DG_Gen} = \sum_{t=1}^{8760} P_{DG_Gen}(t) \quad (58)$$

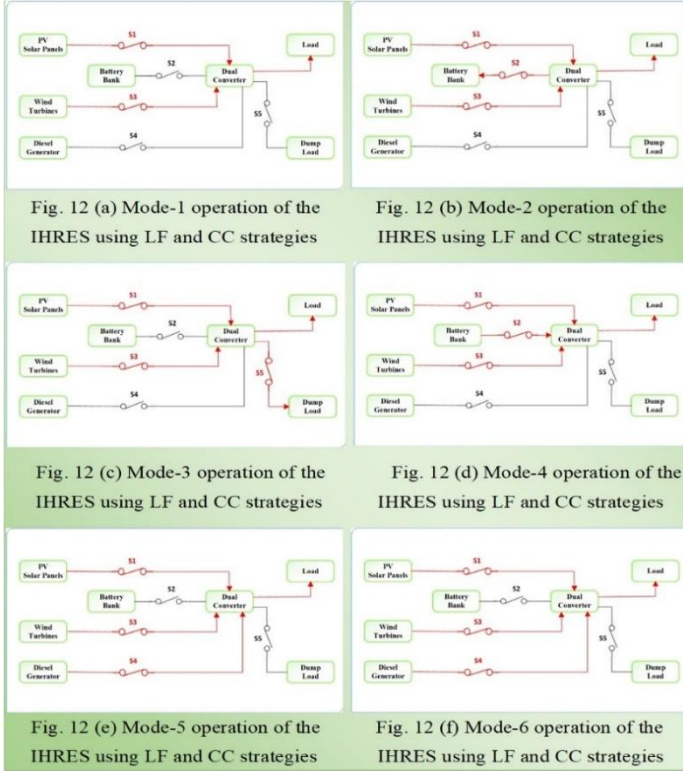


Figure 12: Operating modes of the IHRES using LF and CC strategies

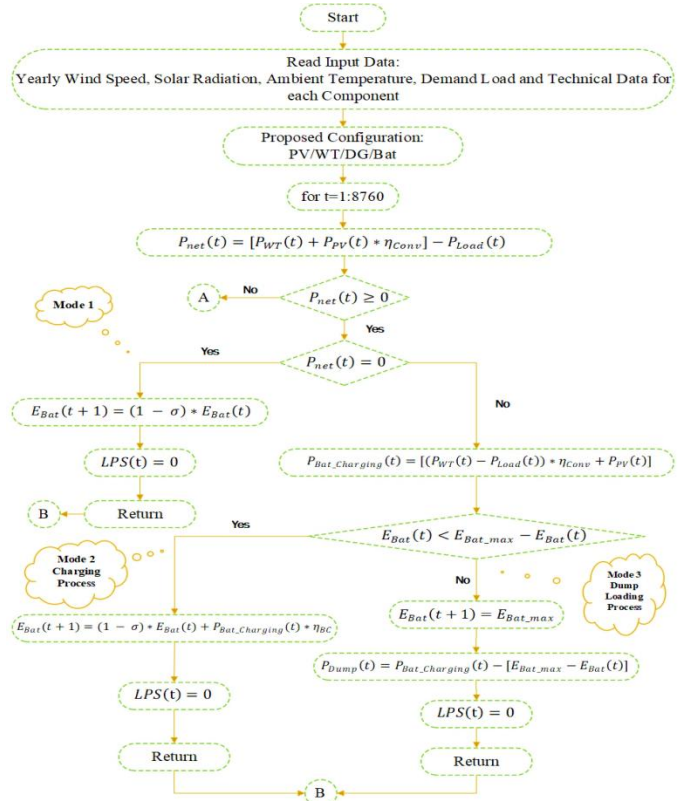


Figure 13: Flowchart of the EMS operating modes and acquisition of LPSP using LF and CC strategies.

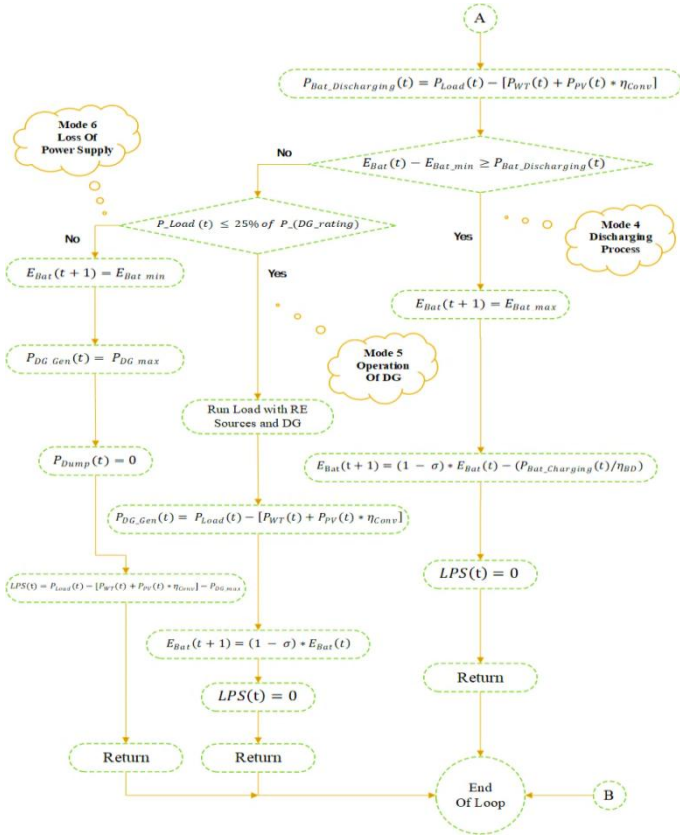


Figure 14: Flowchart of the EMS operating modes and acquisition of LPSP using LF and CC strategies.

5.2. The Proposed Algorithm

Salp swarm method (SSA) is recognized as a member of the metaheuristic family in the literature because of its track record of producing the most globally optimum answers to other current scientific issues. The salp swarm behavior served as the basis for the invention of the SSA by [108].

The salp is a tiny, translucent creature that resembles a jellyfish and has a body structured like a barrel, As Figure 15(a) shows, salps also congregate in the deep ocean as a swarm, like a chain, in order to look for food, as Figure 15(b) shows.

Two groups - a leader and followers - have been identified in the mathematical modeling of the salp chain population. The salp leader leads the other salps to follow behind the chain by standing in front of it. Similar to earlier swarm-based optimization techniques, the salps' placement is described in an n-dimensional search space, where (n) is the number of variables in the suggested objective. In this sense, the salps' locations have been maintained in a two-dimensional matrix called "Z" and it is assumed that the swarm's objective is to reach food source "f" in the search space. The update of the position of the leader may be determined as follows:

$$Z_q^1 = \begin{cases} f_q + [c_1 * ((ul_q - ll_q) * c_2 + ll_q)], & c_3 \geq 0 \\ f_q - [c_1 * ((ul_q - ll_q) * c_2 + ll_q)], & c_3 < 0 \end{cases} \quad (59)$$

where, Z_q^1 indicates the leader salp's position in the q^{th} dimension. The lower and upper bounds of the q^{th} dimension are denoted by ll_q and ul_q . c_1 , c_2 and c_3 are the random numbers.

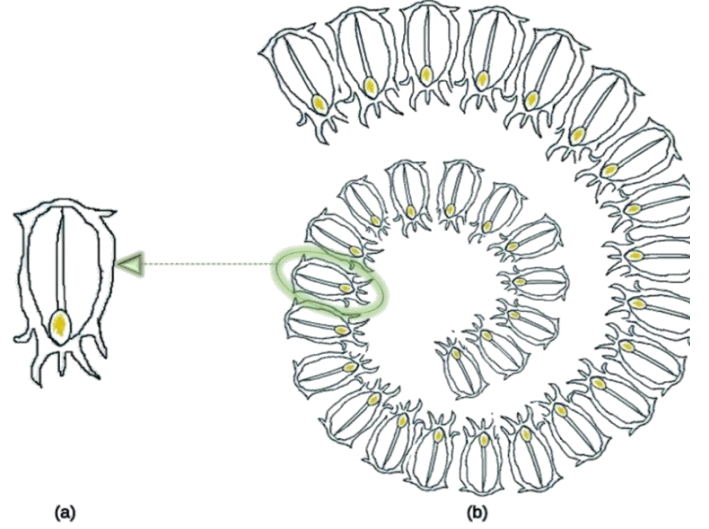


Figure 15: (a) Salp and (b) Salp Swarm Chain.

The leader itself is able to adjust its location based on where the food supply is. The coefficient c_1 , found in next formula, is the most important element in ensuring that exploration and exploitation in SSA are balanced, as the following:

$$c_1 = 2e^{-\left(\frac{4u}{U}\right)^2} \quad (60)$$

where, u and U are the maximum and current numbers of iterations, correspondingly.

The interval [0,1] is where the random integers c_2 and c_3 are created evenly. These parameters specify the step size and which direction the subsequent position in the q^{th} dimension should be in relation to positive or negative infinity. The following formula, which uses Newton's law of motion, can be used to update the followers' location:

$$Z_q^i = \frac{1}{2}at^2 + V_0t \quad (61)$$

where V_0 is the initial speed, t is the time interval, and $i \geq 2$ indicates that Z_q^i is the position of the i^{th} follower salp in the q^{th} dimension and a is the acceleration rate and equals to $a = \frac{V_{final}}{t}$ where $V_{final} = \frac{Z - Z_0}{t}$. An iteration is defined as a time 't'; the difference between two iterations is regarded as 1, and if $V_0 = 0$, Z_q^i is defined as follows:

$$Z_q^i = \frac{1}{2} * (Z_q^i + Z_q^{i-1}) \quad (62)$$

where, Z_q^i indicates the position of the i^{th} follower salp in the q^{th} dimension when $i \geq 2$. By using previous formula the salp chains are simulated.

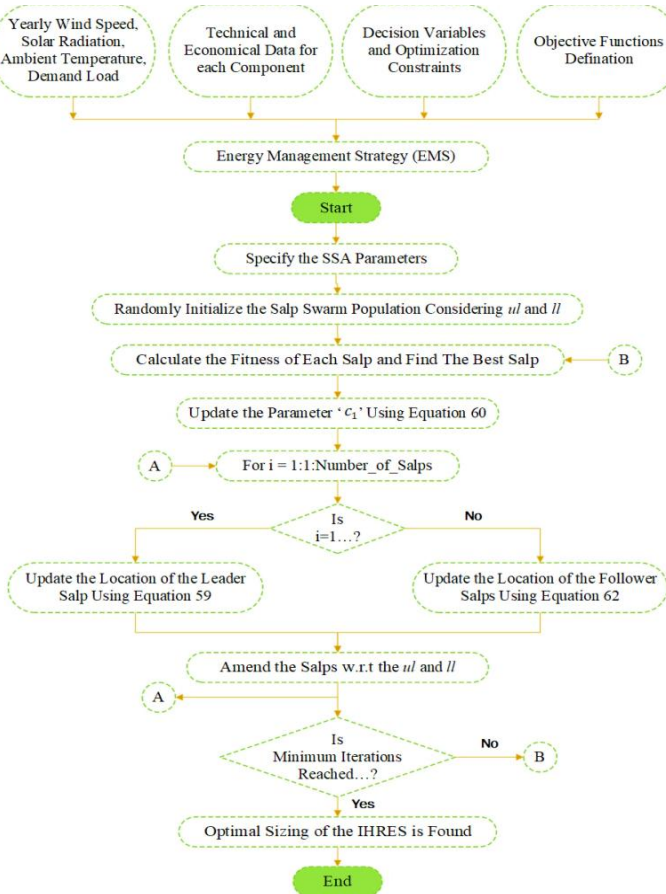


Figure 16: Flowchart illustrating the procedure for evaluating the optimal IHRES sizing with SSA.

The SSA has several benefits, including a straightforward idea, simple implementation, and great efficiency. It also solves optimization issues rapidly by utilizing its fast convergence feature to get the global best optimum values. A comprehensive explanation of the process with SSA which used to determine the ideal IHRES size with the lowest LEC from the most economic WTs and satisfy the permitted limits for $LPSP$ and E_{Dump} . Depending on input data which serve the program is provided in the previous Figure 16, which is a flowchart.

6. Case Study

The Minia governorate's New Minia city in Egypt has been used to evaluate the optimal way to size a small-scale off-grid hybrid RE system. According to the data currently available, the average yearly wind speed in the chosen location is 5.19 m/s at a height of 10 m, and the average daily horizontal solar radiation is 6.05 kWh/m²/day. Table 2 and Table 3 presents the technical parameters of ten WTs from various manufacturers that were employed in this study to deliver the required load, PV system

, battery bank, and DG. In this study, the system lifespan of 25 years has been selected, and the rate of interest is 3.2%.

The simulation program MATLAB was used to get the desired results. We previously talked about the control parameters and the limitations of the optimized variables. The maximum number of search agents is around 30, and the maximum number of iterations was set at 100.

Table 2: The technical parameters of the IHRES

Component	WT No.	Manufacturer	$P_{R,WT}$ (kw)	D (m)	u_{cutin} (m/s)	u_{rated} (m/s)	u_{cutoff} (m/s)	H (m)
Wind Turbines	WT 1	Enercon-1	330	34	3	13	34	50
	WT 2	ACSA_1	225	27	3.5	13.5	25	50
	WT 3	Fuhrlander_3	250	50	2.5	15	25	42
	WT 4	Ecotecnia_2	600	44	4	14.5	25	45
	WT 5	IIP-1	250	30	3	12	25	50
	WT 6	NEPC_3	400	31	4	15	25	36
	WT 7	Southern Wind Farms	225	29.8	4	15	25	45
	WT 8	Enercon_2	330	33.4	3	13	34	37
	WT 9	NEPC_2	250	27.6	4	17	25	45
	WT 10	India Wind Power	250	29.7	3	15	25	50
Component	Parameter	Value	Unit					
Photovoltaic Panels	Model	JKM400M-72H-V						
	Maxpower	400	Watt					
	Length	2008	mm					
	Width	1002	mm					
	Thickness	40	mm					
	Module Efficiency	16.3	%					
	Operating Temperature	-10 : 85	°C					
Temperature Coefficient	0.37	%						

Table 3: The technical parameters of the IHRES

Component	Parameter	Value	Unit
Battery Bank	Model	RS Lead Acid-SSIG 06 490-Battery	
	Nominal Capacity (S_{BAT})	490	Ah
	Nominal Voltage (V_{BAT})	6	Volt
	Round Trip Efficiency (η_{bat})	85	%
	DOD	80	%
	Internal Resistance	< 0.005	Ω
	Operating Temperature	-20 : 45	$^{\circ}C$
	Self-discharge rate (%/day) (σ)	0.2	%
Component	Parameter	Value	Unit
Diesel Generator	Model	DGK125F	
	Phase	3	Ph
	Rated Output	100	Kw
	Frequency	50	Hz
	Power Factor	80	%
	Dry Weight	2990	Kg
	Net Weight	3670	Kg

Table 4 lists the economic parameters for every HRES component. An overview of the $C_{Initial_Capital}$, $C_{O\&M}$, C_{Rep} , C_{Fuel} , $C_{Erection}$ and V_{Scarp} with useful life of HRES components is given in this table.

Table 4: The economic values of the IHRES

Item	WT (kw)	WT Civil Work (kw)	PV (kw)	PV Civil Work (kw)	Battery (kw)	DG (kw)	Dual Converter (kw)
$C_{Initial_Capital}$ (\$)	1500	300	1150	460	220	350	300
$C_{O\&M}$ (%)	3	3	1	1	3	3	Null
C_{Rep} (\$)	1200	Null	Null	Null	176	350	270
V_{Scarp} (%)	20	20	10	20	20	20	10
Salvage Times	2	1	1	1	7	3	3
Lifetime (Year)	20	25	25	25	4	10	10
No. of Replacements	1	0	0	0	6	2	2

6.1. Optimal Combination of The System Components

In order to provide the load requirements for a remote site in the New Minia Governorate of Egypt, the size of the proposed microgrid, which is determined by the number of (i) WTs, (ii) PV modules, (iii) battery banks, and (iv) DG units, has been specified in this study using the SSA method based on MATLAB code.

In addition to matching the load with the available RE sources for decreasing needs for DGs and then COE with high reliability and performance, so DSM strategy is applied step by step in a

flowchart to perform the operation of the microgrid as shown in Figure 17.

Firstly, we represent the COE values for each WT in the case study with the optimization methods for that particular site. It is evident from analysis WT 5 (ITP-1) at SSA yields the lowest COE value. In the ideal scenario, Figure 18 illustrates how the COE changes in relation to the optimization algorithms. The WT system and PV solar panels contribute at SSA in the ideal scenario ($N_{WT} = 78$ WTs, $N_{PV} = 134946$ panels), so based on previous analysis of optimization; Table 5 shows the detailed results of the optimization algorithm SSA compared with other metaheuristic techniques which operated on WT5, while the optimization algorithms were evaluated considering 100 iterations. Figure 19 shows that after 53 iterations, SSA was able to reach the optimal solution of 0.21957 \$/kWh within the specified operation limits. Meanwhile, after 72 iterations, DA reached the best cost of 0.22132 \$/kWh, after 75 iterations, GRO reached the best cost of 0.22009 \$/kWh, after 56 iterations, ALO reached the best cost of 0.22055 \$/kWh, after 58 iterations, PSO reached the best cost of 0.22083 \$/kWh, after 64 iterations, MFO reached the best cost of 0.22134 \$/kWh, and after 58 iterations, WOA reached the best cost of 0.22717 \$/kWh.

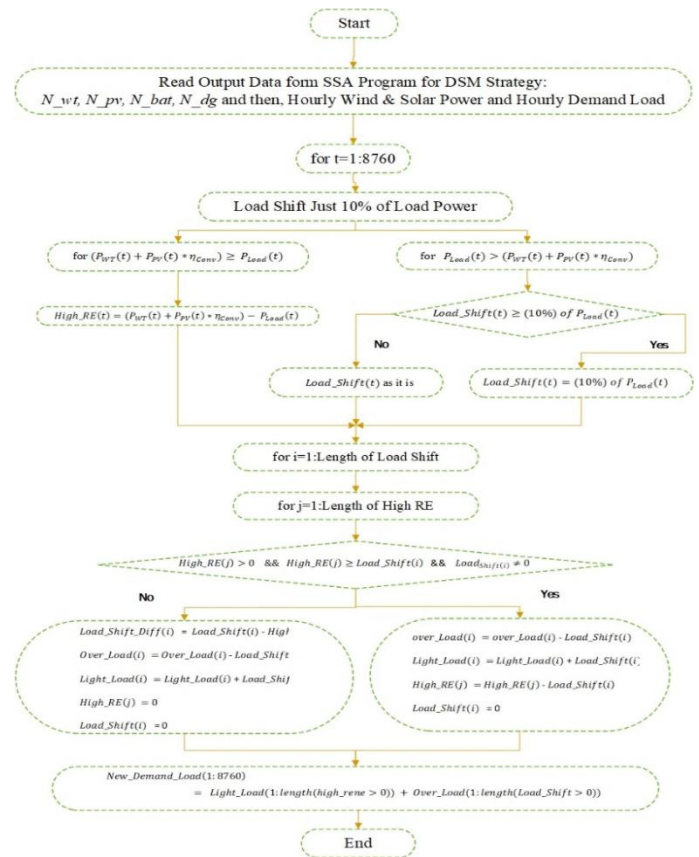


Figure 17: Flowchart illustrating the procedure for applying DSM for the load

The results indicate that, in comparison to alternative methods, the SSA optimization approach may achieve the objective function's minimum best ideal value more quickly and effectively.

Based on the simulation results, it can be concluded that the system with the lowest *TPV* and *LPSP* within the set constraints will have the lowest *COE* predicted by the SSA. Additionally, SSSA projects the optimal *COE* of 0.21975 \$/kWh, which yields a 4.5433×10^8 \$ total present value and ensures the *LPSP* value of 0.499, both of which agree with the predetermined value (≤ 0.05). Unfortunately, none of the suggested methods were able to get the cost function's optimum end value.

fuel consumption and the fuel cost annually. Figure 20 shows the total present value (\$) for all the system during lifetime depending on many optimizations techniques follow.

Table 5: Comparison between optimization algorithm SSA and the others metaheuristic techniques for WT5

Optimization Techniques	WOA	MFO	PSO	ALO	DA	GRO	SSA
Best Objective Function	0.22717	0.22134	0.22083	0.22055	0.22132	0.22009	0.21957
Best Solution	WT	80	79	77	78	79	78
	PV	135410	135343	135117	135253	135016	135006
	Battery	29416	29330	29227	29287	29186	29110
	DG	21	21	21	21	21	21
No. of Iterations for Optimal Solution	58	64	58	56	72	75	53
TPC (\$)	4.6007e8	4.5766e8	4.5657e8	4.5597e8	4.5749e8	4.5502e8	4.5433e8
Dump Load (%)	0.04	0.039	0.04	0.04	0.04	0.039	0.038
LPSP (%)	0.05	0.05	0.049	0.05	0.05	0.05	0.049
Fuel Cost (\$)	1.8314e7	1.8400e7	1.8508e7	1.8546e7	1.8473e7	1.8675e7	1.8829e7

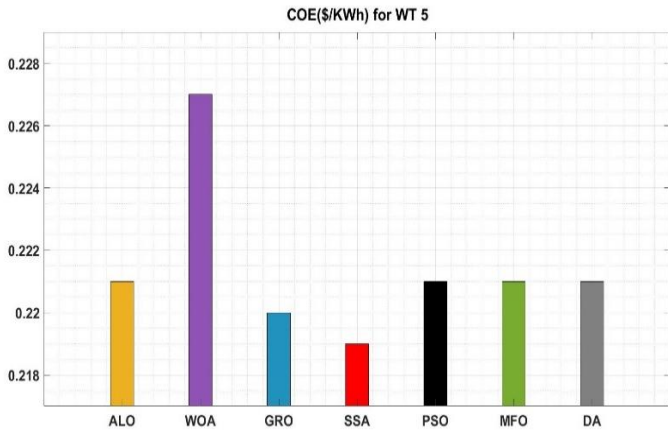


Figure 18: The COE related to the optimization algorithms

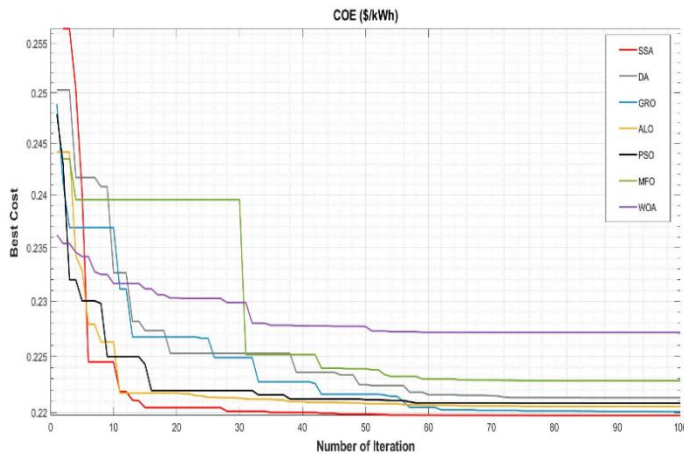


Figure 19: Convergence curves of the proposed optimization techniques

The SSA algorithm estimates 78 WTs, 134946 PV modules, 29056 battery banks, and 21 DG units in order to guarantee the minimal *COE* at the suggested location. Furthermore, the *COE* that SSA was able to get demonstrates that the suggested hybrid microgrid system can provide the remote town with electricity at a reasonable cost. For every optimization strategy, the components of the objective function are shown in **Figure 20** and **Figure 21** such as total present value (*TPV*) and fuel cost, which provides a clear presentation of the comparison.

SSA has the highest gasoline expense even if it offers the lowest *COE*. This can be explained by the fact that SSA specifies the lowest possible number of battery storage units (29056 units), which results in significant initialization and replacement costs. As a result, the *COE* decreases when the quantity of battery storage units is decreased. Conversely, if the storage system's capacity is reduced, the DG must run for a longer period of time, increasing

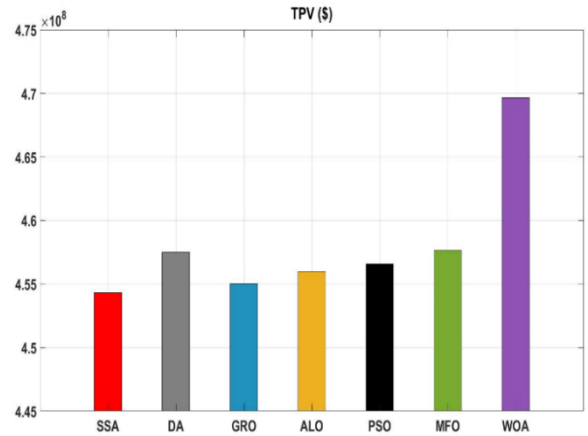


Figure 20: The total present value (\$) for all the system during lifetime

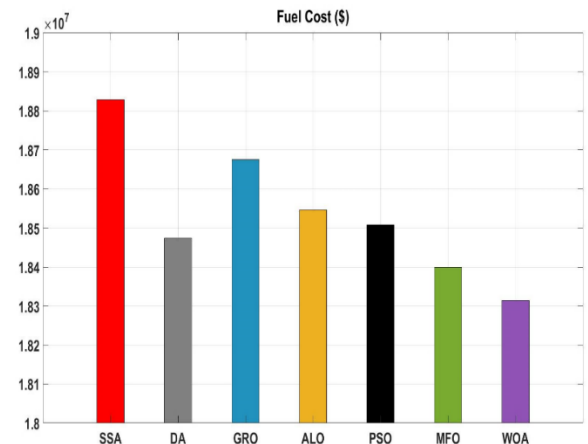


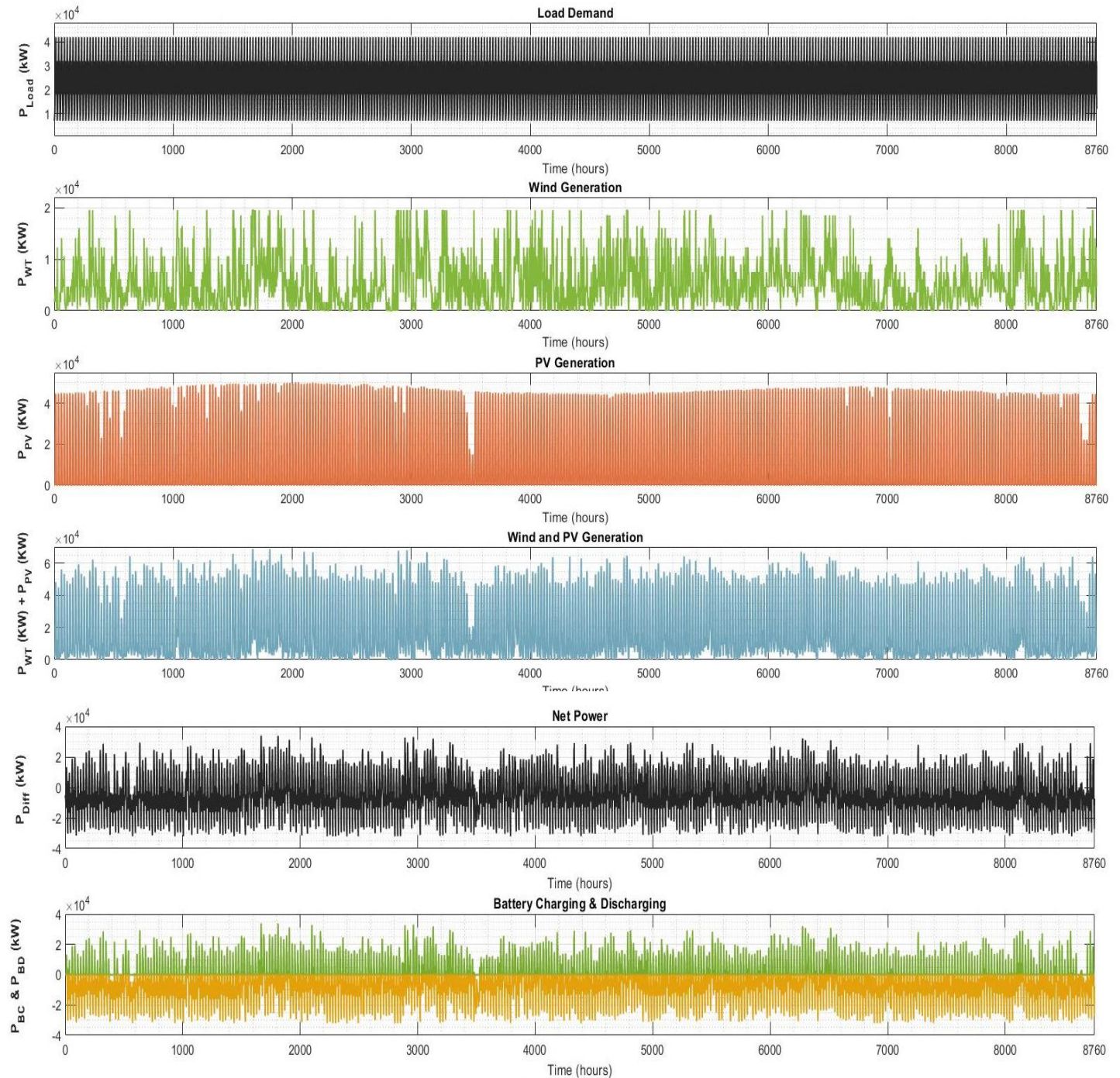
Figure 21: The fuel cost (\$)

6.2. Application of the Optimal Case

The suggested hybrid system's component hourly power variations for the best-case scenario of SSA are depicted in **Figure 22**. The results are shown in this figure as follows: load demand (P_{load}), power produced by PV solar panels, power produced by WTs, and the total power produced by renewable sources ($P_{WT} + P_{PV}$), net power, power of the storage battery system to charge and discharge ($P_{Bat_charging}$ & $P_{Bat_Discharging}$), battery bank system state of charge as a percentage of storage system capacity (SOC), the amount of fuel consumed by the DG units, the number of units

operating each hour (DG units), the dump load power (P_{Dump}), and the $LPSP$.

Given to this area's low wind speed, DG units are regularly run at varying levels of power to meet the load's energy needs during the hours when PV and WT generation is insufficient, and the battery system's state of charge is low (SOC). While the dump load is operating to absorb surplus power over the load's requirement and the storage system's maximum capacity during peak hours of output from renewable sources.



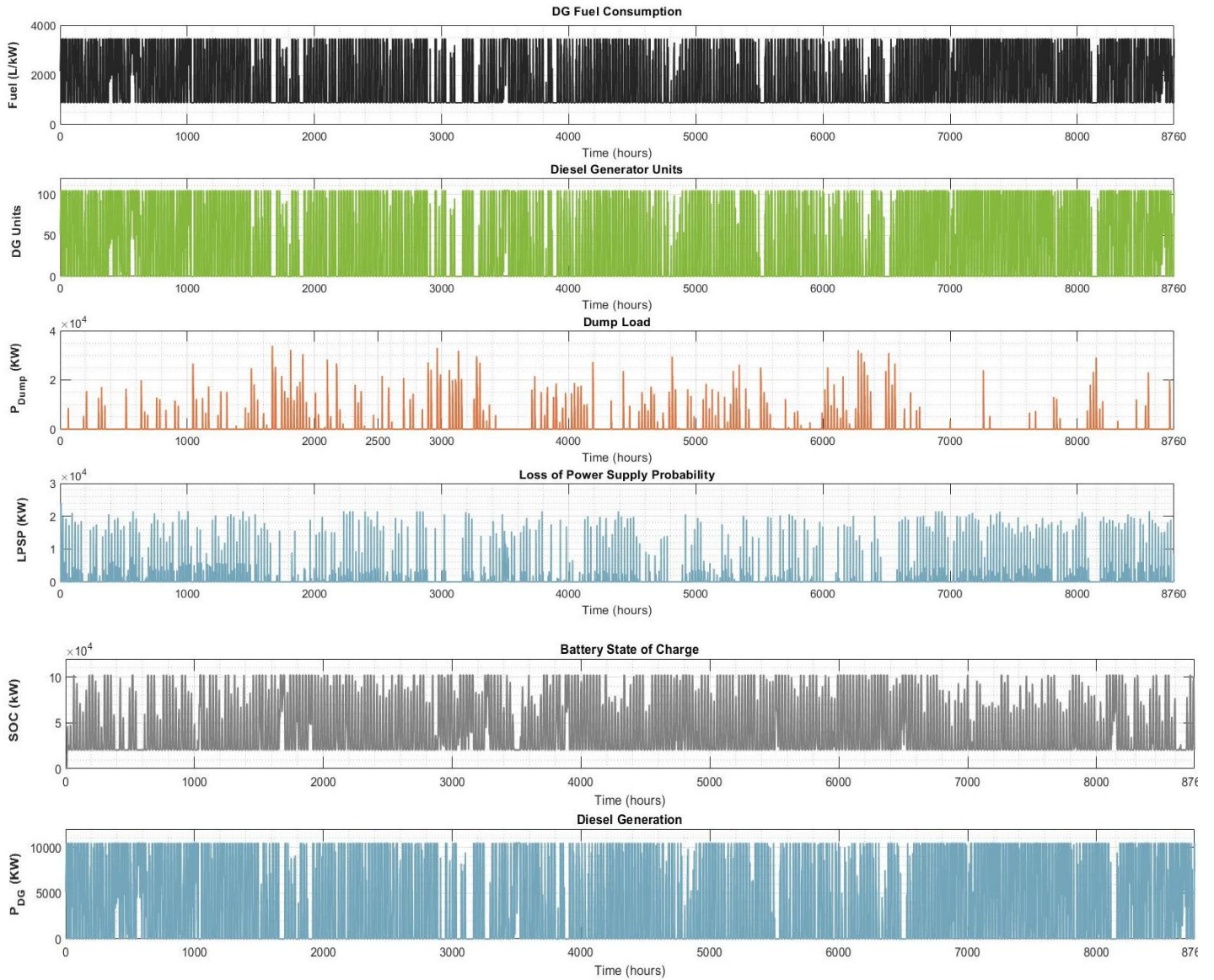


Figure 22: Simulation results of the optimum solution for 8760 hours (i.e., one year) of operation obtained from SSA

As shown in Figure 23, the simulation results for a particular 24-hour period without DSM technique in the optimal case show changes in the power of the load (P_{load}), the power from the WT and PV systems ($P_{WT} + P_{PV}$), the storage battery system's capacity to charge and discharge ($P_{Bat_charging}$ & $P_{Bat_Discharging}$), the output power from the DG (P_{DG}), the dump load power (P_{Dump}), and the LPSP. This serves as an example to help understand the reasoning behind the suggested optimization algorithm. It is obvious that there are two peaks on the daily load curve.

The first peak occurs at around 1:00pm, when the temperature is quite high, and air conditioning is required to lower the temperature. The second peak occurs after dusk, at around 6:00pm. During the night and early morning, the DG runs continuously

since RE sources produce less electricity at these periods. The DG is turned off when the electricity produced by unconventional sources exceeds the demand from the load. Thus, the battery banks are charged using the extra power.

Also as shown in Figure 24, the simulation results for a particular 24-hour period with applying DSM technique for 10% of load shifting in the optimal case where the COE has decreased from 0.2196 to 0.2179 (\$/KWh). Where this shifting clip overload (regions of deficit energy) and distribute it on regions of surplus energy and load curve become flexible to add or clip. So, the amount of dummy energy produced by a fully charged battery and battery bank storage system reduce the requirement for a backup DG. Consequently, overall cost of the system decreased.

After applying DSM all changes in the power of the load (P_{load}), the power from the WT and PV systems ($P_{WT} + P_{PV}$), the storage battery system's capacity to charge and discharge ($P_{Bat_charging}$ & $P_{Bat_Discharging}$), the output power from the DG (P_{DG}), the dump load power (P_{Dump}), and the LPSP will be shown.

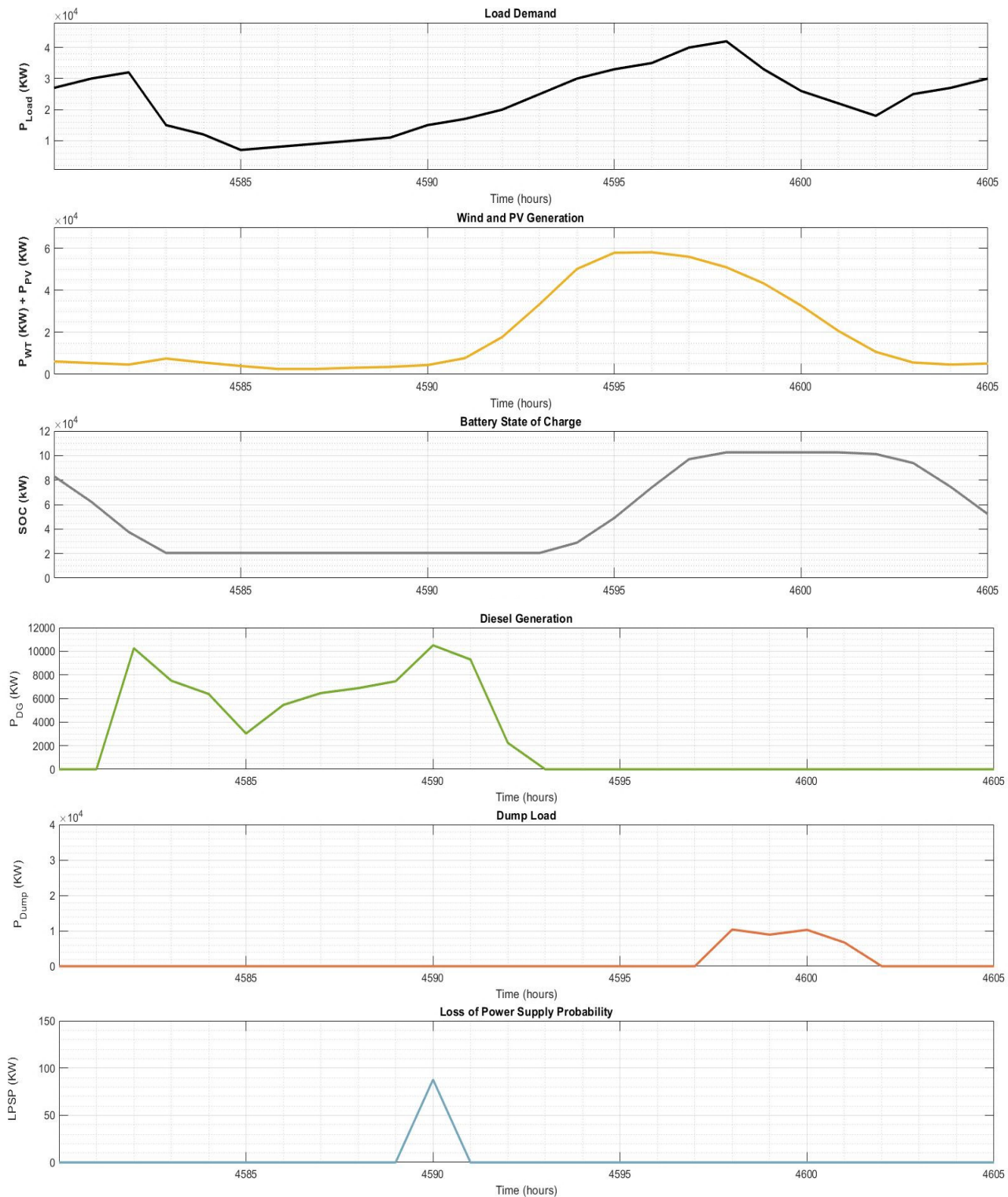


Figure 23: Simulation results for just one day of operation (24 hours) of the optimum solution derived from SSA without using DSM

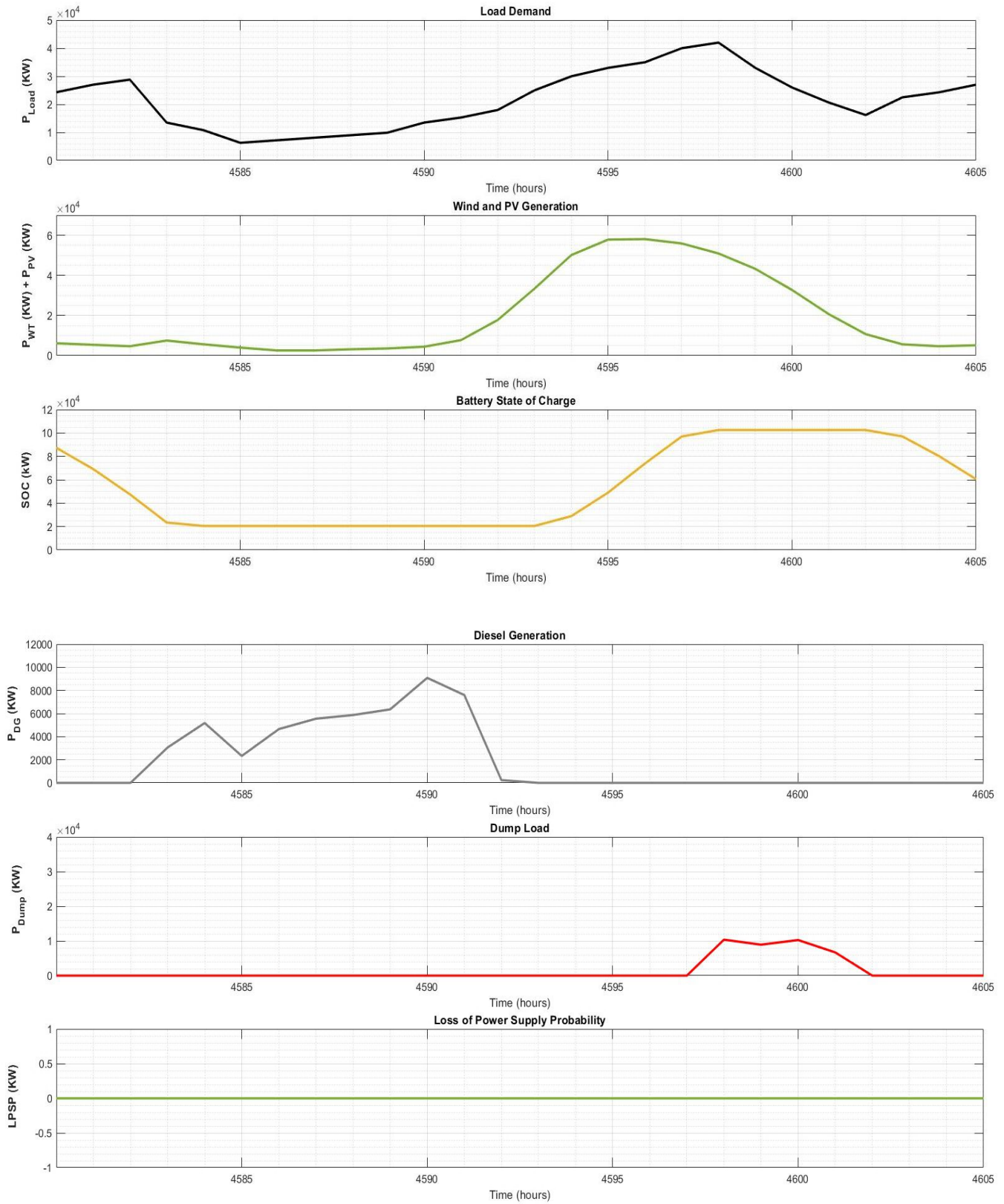


Figure 24: Simulation results of the optimum possible solution, derived from SSA, using a 10% load-shifting DSM method over a full day of operation (24 hours)

In addition, as shown in Figure 25, the simulation results for a particular 24-hour period with DSM technique for 80% of load shifting in the optimal case where the *COE* has decreased from 0.2196 to 0.2013 (\$/KWh).

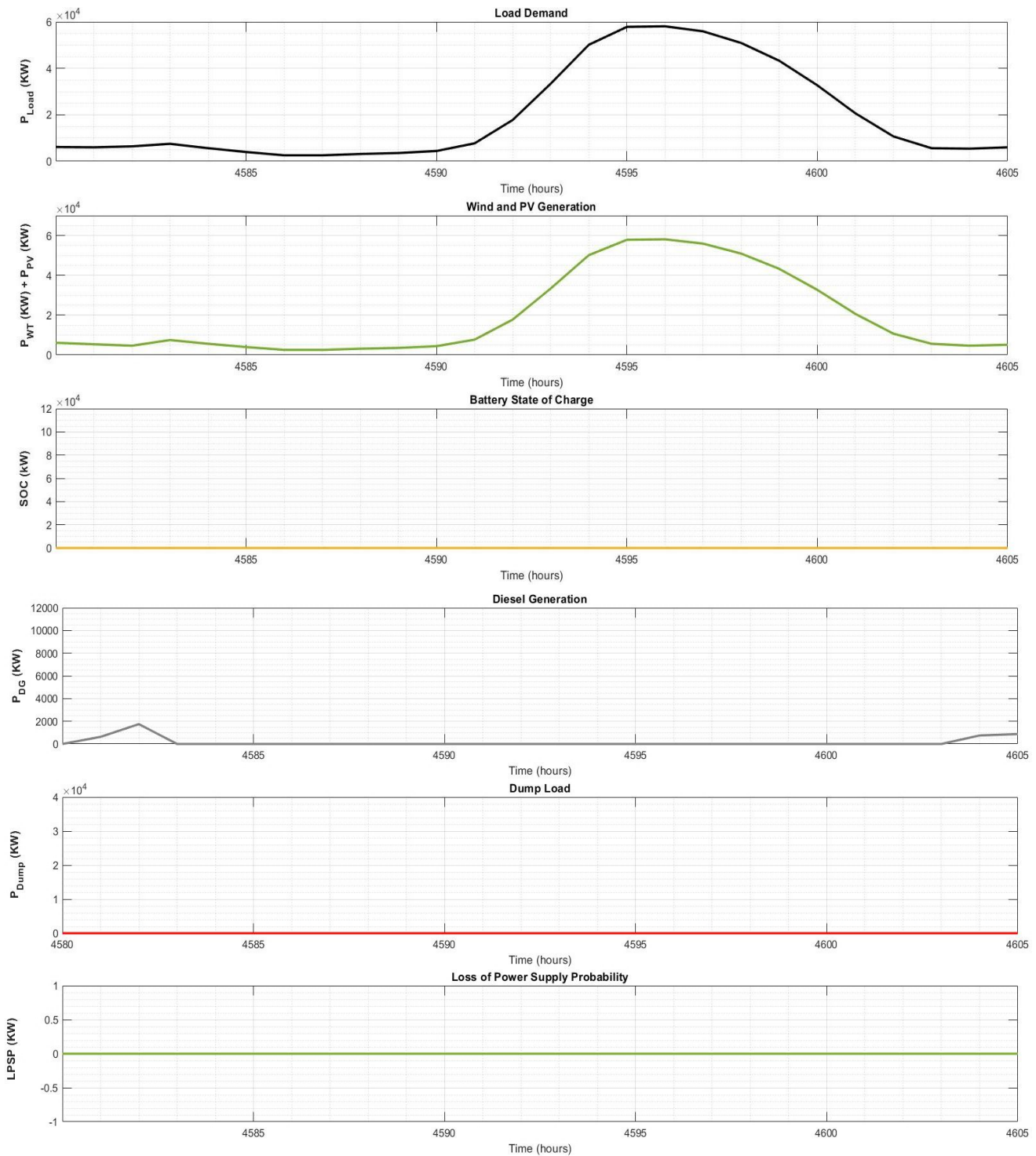


Figure 25: Simulation results of the optimum possible solution, derived from SSA, using a 80% load-shifting DSM method over a full day of operation (24 hours)

The previous figures show changes in the power of the load (P_{load}), the power from the WT and PV systems ($P_{WT} + P_{PV}$), the storage battery system's capacity to charge and discharge ($P_{Bat_charging}$ & $P_{Bat_Discharging}$), the power output of the DG (P_{DG}), the dump load power (P_{Dump}), and the LPSP.

By using the DSM strategy with its efficient techniques, the total system cost is reduced as shown in **Figure 26**, because this strategy tries to match the demand load with available RE sources, so only a small number of backup DGs are needed to cover up for the lost power hours, and then small number of battery bank which store surplus power, consequently reducing the LPSP and dump energy.

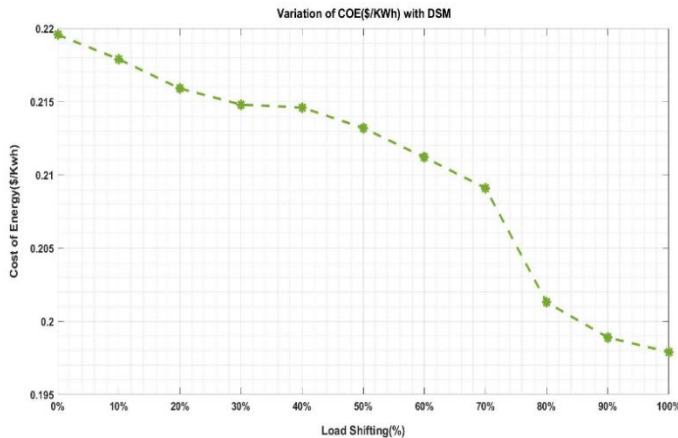


Figure 26: The COE (\$/KWh) with load shifting percentage (%)

7. Conclusion

In this paper, a new, high-performed program has been developed with participation of multi-metaheuristic algorithms in addition to an effective strategy such as LF, CC and DSM techniques for the sizing and optimization of isolated integrated hybrid WT/PV/DG/battery bank energy systems to feed loads in remote area of New Minia city located in Egypt considering uncertainty analysis of natural sources (sun and wind) and economic changes based on site-specific weather data and real-time information. To increase the system's reliability and efficiency, the IHRES's units are connected via hybrid DC and AC buses. Once the batteries were completely charged, a dummy load was employed to absorb the surplus power in the system.

Seven metaheuristic optimization approaches, including WOA, MFO, PSO, ALO, DA, GRO, and SSA, were used to identify the optimal configuration for a standalone hybrid RE system. After a thorough comparative analysis, it is shown that SSA had the best speed of convergence and the highest operating efficiency to get the global best optimum values. This case study can actually help the decision makers in Egypt's New Minia city consider the usage of hybrid systems as a practical electrification option that can help them to reduce dependency on traditional fossil fuels resources.

This flexible program has the availability to estimate the optimal size of the proposed IHRES and achieved the main objective function of this program, which is determining optimum size of the design parameter N_{WT} , N_{PV} , capacity of DG and battery bank to meet demand while generating electricity at the

lowest possible cost COE , minimum $LPSP$ which about 5%, minimum amount of greenhouse gases and minimum amount of dummy which scored 4% of total demand load energy at highest reliability and performance. The following is an overview of these results:

- Introducing high-performance metaheuristic algorithms that surpass both conventional deterministic approaches and all commercial software in solving hybrid RE system design problems.
- Presenting a successful optimization technique SSA with comparatively minimal computing needs. SSA can achieve the global optimum, which in this case is represented by the lowest cost. Furthermore, it is observed that using SSA results in less iterations needed to get the ideal solution than other methods. In addition, the outcomes proved that the SSA method could be used quickly and with great performance.
- Investigation of the multi-objective function suggested in this paper, which identifies the ideal size for every part of a standalone hybrid PV, WT, DG, and battery energy system by evaluating the amount of dummy energy at maximum performance and reliability, the lowest possible COE produced and the loss of a power supply probability (LPSP). The functioning of the system was significantly improved as a consequence.
- Using efficient strategies like DSM which decreased the COE from 0.21957 to 0.2159 (\$/KWh) with applying load shifting of 20%, LF, CC, and energy conservation with various techniques like load shifting, peak clipping, energy conservation, valley filling, flexible load shape, and load building. These strategies have a major impact on meeting load demand and lowering the size of system components, which directly decreased the LCC.
- Representing the uncertainty analysis which describes the intermittent nature of solar and wind and its effect on generated power from WTs and PV solar panels.

7.1. Recommendations for Further Work

There are several possible paths for the research work that this paper describes. The following highlights the most promising expansions of the work that this paper presents:

- The capacity of unit DG the largest it be can, the efficient system is developed and then the minimum total cost, because increasing the DG capacity directly decreasing the total number of required DG units which decreasing the regular maintenance, initial capital cost and increasing performance of the system.
- The battery bank replacement will be necessary several times during the system's lifetime due to its limited lifespan in comparison to the other IHRES components. Furthermore, it represents an important portion of the project's overall costs. Finding a longer-term and more affordable energy storage solution than battery storage is therefore important.
- Selecting the most economical system design after taking into account a number of the IHRES independent power

generation configurations, such as solar PV panels, WT, DG, FC, hydrogen tanks, and storage batteries.

References

1. S. Mansour, M. Alahmadi, P. M. Atkinson, and A. Dewan, "Forecasting of built-up land expansion in a desert urban environment," *Remote Sens.*, vol. 14, no. 9, p. 2037, 2022, <https://doi.org/10.3390/rs14092037>.
2. R. E. S. Abdel-Galil, "Desert reclamation, a management system for sustainable urban expansion," *Prog. Plann.*, vol. 78, no. 4, pp. 151–206, 2012, <https://doi.org/10.1016/j.progress.2012.04.003>.
3. M. E. Gabr, "Land reclamation projects in the Egyptian Western Desert: Management of 1.5 million acres of groundwater irrigation," *Water Int.*, vol. 48, no. 2, pp. 240–258, 2023, <https://doi.org/10.1080/02508060.2023.2185745>.
4. Mohamed, Mohamed A., et al. "Multi-agent based optimal sizing of hybrid renewable energy systems and their significance in sustainable energy development." *Energy Reports* 12 (2024): 4830-4853. <https://doi.org/10.1016/j.egyrs.2024.10.051>
5. Farh, Hassan M. Hussein, et al. "Optimization and uncertainty analysis of hybrid energy systems using Monte Carlo simulation integrated with genetic algorithm." *Computers and Electrical Engineering* 120 (2024): 109833. <https://doi.org/10.1016/j.compeleceng.2024.109833>.
6. H. Dibaba, I. Demidov, E. Vanadzina, S. Honkapuro, and A. Pinomaa, "Feasibility of rural electrification and connectivity—A methodology and case study," *Appl. Energy*, vol. 315, p. 119013, 2022, <https://doi.org/10.1016/j.apenergy.2022.119013>.
7. F. Rinaldi, F. Moghaddampoor, B. Najafi, and R. Marchesi, "Economic feasibility analysis and optimization of hybrid renewable energy systems for rural electrification in Peru," *Clean Technol. Environ. Policy*, vol. 23, pp. 731–748, 2021, <https://doi.org/10.1007/s10098-020-01906-y>.
8. A. Kalair, N. Abas, M. S. Saleem, A. R. Kalair, and N. Khan, "Role of energy storage systems in energy transition from fossil fuels to renewables," *Energy Storage*, vol. 3, no. 1, p. e135, 2021, <https://doi.org/10.1002/est2.135>.
9. B. Li and N. Haneklaus, "The role of renewable energy, fossil fuel consumption, urbanization and economic growth on CO₂ emissions in China," *Energy Reports*, vol. 7, pp. 783–791, 2021, <https://doi.org/10.1016/j.egyrs.2021.09.194>.
10. M. K. Anser, I. Hanif, M. Alharthi, and I. S. Chaudhry, "Impact of fossil fuels, renewable energy consumption and industrial growth on carbon emissions in Latin American and Caribbean economies," *Atmosfera*, vol. 33, no. 3, pp. 201–213, 2020, <https://doi.org/10.20937/atm.52732>.
11. R. M. Hannun and A. H. A. Razzaq, "Air pollution resulted from coal, oil and gas firing in thermal power plants and treatment: a review," in *IOP Conference Series: Earth and Environmental Science*, IOP Publishing, 2022, p. 012008, <https://doi.org/10.1088/1755-1315/1002/1/012008>.
12. Y. Majeed et al., "Renewable energy as an alternative source for energy management in agriculture," *Energy Reports*, vol. 10, pp. 344–359, 2023, <https://doi.org/10.1016/j.egyrs.2023.06.032>.
13. M. M. Maroto-Valer, C. Song, and Y. Soong, *Environmental challenges and greenhouse gas control for fossil fuel utilization in the 21st century*. Springer Science & Business Media, 2012, <https://doi.org/10.1007/978-1-4615-0773-4>.
14. K. O. Yoro and M. O. Daramola, "CO₂ emission sources, greenhouse gases, and the global warming effect," in *Advances in carbon capture*, Elsevier, 2020, pp. 3–28, <https://doi.org/10.1016/B978-0-12-819657-1.00001-3>.
15. W. Wang, L. W. Fan, and P. Zhou, "Evolution of global fossil fuel trade dependencies," *Energy*, vol. 238, p. 121924, 2022, <https://doi.org/10.1016/j.energy.2021.121924>.
16. X. Hu, "RETRACTED: Green economic recovery in Central Asia by utilizing natural resources," 2023, Elsevier, <https://doi.org/10.1016/j.resourpol.2023.103582>.
17. P. A. Østergaard, N. Duic, Y. Noorollahi, H. Mikulcic, and S. Kalogirou, "Sustainable development using renewable energy technology," 2020, Elsevier, <https://doi.org/10.1016/j.renene.2019.08.094>.
18. P. Dechamps, "The IEA World Energy Outlook 2022—a brief analysis and implications," *Eur. Energy Clim. J.*, vol. 11, no. 3, pp. 100–103, 2023, <https://doi.org/10.4337/eej.2023.03.05>.
19. S. Asiaban et al., "Wind and solar intermittency and the associated integration challenges: A comprehensive review including the status in the Belgian power system," *Energies*, vol. 14, no. 9, p. 2630, 2021, <https://doi.org/10.3390/en14092630>.
20. A. A. Abou El-Ela, R. A. El-Schiemy, S. M. Allam, A. M. Shaheen, N. A. Nagem, and A. M. Sharaf, "Renewable energy micro-grid interfacing: economic and environmental issues," *Electronics*, vol. 11, no. 5, p. 815, 2022, <https://doi.org/10.3390/electronics11050815>.
21. T. M. Aljohani, A. F. Ebrahim, and O. Mohammed, "Hybrid microgrid energy management and control based on metaheuristic-driven vector-decoupled algorithm considering intermittent renewable sources and electric vehicles charging lot," *Energies*, vol. 13, no. 13, p. 3423, 2020, <https://doi.org/10.3390/en13133423>.
22. G. Suresh, D. Prasad, and M. Gopila, "An efficient approach based power flow management in smart grid system with hybrid renewable energy sources," *Renew. Energy Focus*, vol. 39, pp. 110–122, 2021, <https://doi.org/10.1016/j.ref.2021.07.009>.
23. M. Grimm, L. Lenz, J. Peters, and M. Sievert, "Demand for off-grid solar electricity: Experimental evidence from Rwanda," *J. Assoc. Environ. Resour. Econ.*, vol. 7, no. 3, pp. 417–454, 2020, <https://doi.org/10.1086/707384>.
24. B. K. Das, M. A. Alotaibi, P. Das, M. S. Islam, S. K. Das, and M. A. Hossain, "Feasibility and techno-economic analysis of stand-alone and grid-connected PV/Wind/Diesel/Batt hybrid energy system: A case study," *Energy Strateg. Rev.*, vol. 37, p. 100673, 2021, <https://doi.org/10.1016/j.esr.2021.100673>.
25. A. M. Eltamaly and A. A. Al-Shamma'a, "Optimal configuration for isolated hybrid renewable energy systems," *J. Renew. Sustain. Energy*, vol. 8, no. 4, 2016, <https://doi.org/10.1063/1.4960407>.
26. L. K. Gan, J. K. H. Shek, and M. A. Mueller, "Hybrid wind–photovoltaic–diesel–battery system sizing tool development using empirical approach, life-cycle cost and performance analysis: A case study in Scotland," *Energy Convers. Manag.*, vol. 106, pp. 479–494, 2015, <https://doi.org/10.1016/j.enconman.2015.09.029>.
27. Monteiro, Amanda, et al. "Development of a Tool for Sizing and Technical–Financial Analysis of Energy-Storage Systems Using Batteries." *Energy Technology* 12.5 (2024): 2301638. <https://doi.org/10.1002/ente.202301638>
28. A. Tiwary, S. Spasova, and I. D. Williams, "A community-scale hybrid energy system integrating biomass for localised solid waste and renewable energy solution: Evaluations in UK and Bulgaria," *Renew. Energy*, vol. 139, pp. 960–967, 2019, <https://doi.org/10.1016/j.renene.2019.02.129>.
29. S. Upadhyay and M. P. Sharma, "Development of hybrid energy system with cycle charging strategy using particle swarm optimization for a remote area in India," *Renew. Energy*, vol. 77, pp. 586–598, 2015, <https://doi.org/10.1016/j.renene.2014.12.051>.
30. D. Parra et al., "An interdisciplinary review of energy storage for communities: Challenges and perspectives," *Renew. Sustain. Energy Rev.*, vol. 79, pp. 730–749, 2017, <https://doi.org/10.1016/j.rser.2017.05.003>.
31. M. A. Mohamed, A. M. Eltamaly, A. I. Alolah, and A. Y. Hatata, "A novel framework-based cuckoo search algorithm for sizing and optimization of grid-independent hybrid renewable energy systems," *Int. J. Green Energy*, vol. 16, no. 1, pp. 86–100, 2019, <https://doi.org/10.1080/15435075.2018.1533837>.
32. T. Khatib, I. A. Ibrahim, and A. Mohamed, "A review on sizing methodologies of photovoltaic array and storage battery in a standalone photovoltaic system," *Energy Convers. Manag.*, vol. 120, pp. 430–448, 2016, <https://doi.org/10.1016/j.enconman.2016.05.011>.
33. P. Kumar and S. Deokar, "Designing and simulation tools of renewable energy systems: review literature," *Prog. Adv. Comput. Intell. Eng. Proc. ICACIE* 2016, Vol. 1, pp. 315–324, 2018, https://doi.org/10.1007/978-981-10-6872-0_29.
34. H. Shamachurn, "Optimization of an off-grid domestic Hybrid Energy System in suburban Paris using iHOGA software," *Renew. Energy Focus*, vol. 37, pp. 36–49, 2021, <https://doi.org/10.1016/j.ref.2021.02.004>.
35. A. Mills and S. Al-Hallaj, "Simulation of hydrogen-based hybrid systems using Hybrid2," *Int. J. Hydrogen Energy*, vol. 29, no. 10, pp. 991–999, 2004, <https://doi.org/10.1016/j.ijhydene.2004.01.004>.
36. H. J. Green and J. Manwell, "HYBRID2—A versatile model of the performance of hybrid power systems," National Renewable Energy Lab.(NREL), Golden, CO (United States), 1995, <https://www.osti.gov/biblio/46678>.
37. D. Kaur and P. S. Cheema, "Software tools for analyzing the hybrid renewable energy sources:-a review," in 2017 International Conference on Inventive Systems and Control (ICISC), IEEE, 2017, pp. 1–4, <http://doi.org/10.1109/ICISC.2017.8068591>.
38. S. Sinha and S. S. Chandel, "Review of software tools for hybrid renewable energy systems," *Renew. Sustain. Energy Rev.*, vol. 32, pp. 192–205, 2014, <https://doi.org/10.1016/j.rser.2014.01.035>.
39. M. Baneshi and F. Hadianfard, "Techno-economic feasibility of hybrid

- diesel/PV/wind/battery electricity generation systems for non-residential large electricity consumers under southern Iran climate conditions,” *Energy Convers. Manag.*, vol. 127, pp. 233–244, 2016, <https://doi.org/10.1016/j.enconman.2016.09.008>.
40. J. S. Stein and G. T. Klise, “Models used to assess the performance of photovoltaic systems,” Sandia National Laboratories (SNL), Albuquerque, NM, and Livermore, CA ..., 2009, <https://doi.org/10.2172/974415>.
 41. L. Kendrick, J. Pihl, I. Weinstock, D. Meiners, and D. Trujillo, “Hybrid generation model simulator (HybSim),” SAND2003-3790A, Sandia Natl. Lab. Albuquerque, NM, 2003, <https://doi.org/10.1201/9781003133094>.
 42. A. Fiksel, J. W. Thornton, S. A. Klein, and W. A. Beckman, “Developments to the TRNSYS simulation program,” 1995, <https://doi.org/10.1115/1.2870836>.
 43. S. A. Kalogirou, “Use of TRNSYS for modelling and simulation of a hybrid pv–thermal solar system for Cyprus,” *Renew. energy*, vol. 23, no. 2, pp. 247–260, 2001, [https://doi.org/10.1016/S0960-1481\(00\)00176-2](https://doi.org/10.1016/S0960-1481(00)00176-2).
 44. E. A. Aronson, D. L. Caskey, and B. C. Caskey, “SOLSTOR description and user’s guide,” Sandia National Lab.(SNL-NM), Albuquerque, NM (United States), 1981. [Online]. Available: https://digital.library.unt.edu/ark:/67531/metadc944624/m2/1/high_res_d/rep.ort.pdf, <https://doi.org/10.2172/6551776>.
 45. A. Madhlopa, D. Sparks, S. Keen, M. Moorlach, P. Krog, and T. Dlamini, “Optimization of a PV–wind hybrid system under limited water resources,” *Renew. Sustain. Energy Rev.*, vol. 47, pp. 324–331, 2015, <https://doi.org/10.1016/j.rser.2015.03.051>.
 46. C. E. C. Nogueira et al., “Sizing and simulation of a photovoltaic-wind energy system using batteries, applied for a small rural property located in the south of Brazil,” *Renew. Sustain. Energy Rev.*, vol. 29, pp. 151–157, 2014, <https://doi.org/10.1016/j.rser.2013.08.071>.
 47. W. H. Liu, S. R. W. Alwi, H. Hashim, J. S. Lim, N. E. M. Rozali, and W. S. Ho, “Sizing of Hybrid Power System with varying current type using numerical probabilistic approach,” *Appl. Energy*, vol. 184, pp. 1364–1373, 2016, <https://doi.org/10.1016/j.apenergy.2016.06.035>.
 48. S. M. Zahrae, M. K. Assadi, and R. Saidur, “Application of artificial intelligence methods for hybrid energy system optimization,” *Renew. Sustain. Energy Rev.*, vol. 66, pp. 617–630, 2016, <https://doi.org/10.1016/j.rser.2016.08.028>.
 49. M. A. M. Ramli, H. Bouchekara, and A. S. Alghamdi, “Optimal sizing of PV/wind/diesel hybrid microgrid system using multi-objective self-adaptive differential evolution algorithm,” *Renew. energy*, vol. 121, pp. 400–411, 2018, <https://doi.org/10.1016/j.renene.2018.01.058>.
 50. A. Fathy, “A reliable methodology based on mine blast optimization algorithm for optimal sizing of hybrid PV-wind-FC system for remote area in Egypt,” *Renew. energy*, vol. 95, pp. 367–380, 2016, <https://doi.org/10.1016/j.renene.2016.04.030>.
 51. Z. Shi, R. Wang, and T. Zhang, “Multi-objective optimal design of hybrid renewable energy systems using preference-inspired coevolutionary approach,” *Sol. energy*, vol. 118, pp. 96–106, 2015, <https://doi.org/10.1016/j.solener.2015.03.052>.
 52. A. Maleki and A. Askarzadeh, “Artificial bee swarm optimization for optimum sizing of a stand-alone PV/WT/FC hybrid system considering LPSP concept,” *Sol. Energy*, vol. 107, pp. 227–235, 2014, <https://doi.org/10.1016/j.solener.2014.05.016>.
 53. B. K. Panigrahi, V. R. Pandi, R. Sharma, S. Das, and S. Das, “Multiobjective bacteria foraging algorithm for electrical load dispatch problem,” *Energy Convers. Manag.*, vol. 52, no. 2, pp. 1334–1342, 2011, <https://doi.org/10.1016/j.enconman.2010.09.031>.
 54. A. Giallanza, M. Porretto, G. L. Puma, and G. Marannano, “A sizing approach for stand-alone hybrid photovoltaic-wind-battery systems: A Sicilian case study,” *J. Clean. Prod.*, vol. 199, pp. 817–830, 2018, <https://doi.org/10.1016/j.jclepro.2018.07.223>.
 55. R. A. Gupta, R. Kumar, and A. K. Bansal, “BBO-based small autonomous hybrid power system optimization incorporating wind speed and solar radiation forecasting,” *Renew. Sustain. Energy Rev.*, vol. 41, pp. 1366–1375, 2015, <https://doi.org/10.1016/j.rser.2014.09.017>.
 56. A. Bouaouda and Y. Sayouti, “Hybrid meta-heuristic algorithms for optimal sizing of hybrid renewable energy system: a review of the state-of-the-art,” *Arch. Comput. Methods Eng.*, vol. 29, no. 6, pp. 4049–4083, 2022, <https://doi.org/10.1007/s11831-022-09730-x>.
 57. J. L. Bernal-Agustín, R. Dufo-López, and D. M. Rivas-Ascaso, “Design of isolated hybrid systems minimizing costs and pollutant emissions,” *Renew. Energy*, vol. 31, no. 14, pp. 2227–2244, 2006, <https://doi.org/10.1016/j.renene.2005.11.002>.
 58. R. Dufo-López et al., “Multi-objective optimization minimizing cost and life cycle emissions of stand-alone PV–wind–diesel systems with batteries storage,” *Appl. Energy*, vol. 88, no. 11, pp. 4033–4041, 2011, <https://doi.org/10.1016/j.apenergy.2011.04.019>.
 59. H. Yang, W. Zhou, L. Lu, and Z. Fang, “Optimal sizing method for stand-alone hybrid solar–wind system with LPSP technology by using genetic algorithm,” *Sol. energy*, vol. 82, no. 4, pp. 354–367, 2008, <https://doi.org/10.1016/j.solener.2007.08.005>.
 60. B. O. Bilal, V. Sambou, P. A. Ndiaye, C. M. F. Kébé, and M. Ndong, “Optimal design of a hybrid solar–wind–battery system using the minimization of the annualized cost system and the minimization of the loss of power supply probability (LPSP),” *Renew. Energy*, vol. 35, no. 10, pp. 2388–2390, 2010, <https://doi.org/10.1016/j.renene.2010.03.004>.
 61. S. M. M. Tafreshi, H. A. Zamani, S. M. Ezzati, M. Baghdadi, and H. Vahedi, “Optimal unit sizing of distributed energy resources in microgrid using genetic algorithm,” in 2010 18th Iranian conference on electrical engineering, IEEE, 2010, pp. 836–841, <http://doi.org/10.1109/IRANIANCEE.2010.5506961>.
 62. M. Pirhaghshenasvali and B. Asaei, “Optimal modeling and sizing of a practical hybrid wind/PV/diesel generation system,” in The 5th Annual International Power Electronics, Drive Systems and Technologies Conference (PEDSTC 2014), IEEE, 2014, pp. 506–511.
 63. M. Bashir and J. Sadeh, “Optimal sizing of hybrid wind/photovoltaic/battery considering the uncertainty of wind and photovoltaic power using Monte Carlo,” in 2012 11th international conference on environment and electrical engineering, IEEE, 2012, pp. 1081–1086, <http://doi.org/10.1109/PEDSTC.2014.6799427>.
 64. A. Navaeefard, S. M. M. Tafreshi, M. Barzegari, and A. J. Shahrood, “Optimal sizing of distributed energy resources in microgrid considering wind energy uncertainty with respect to reliability,” in 2010 IEEE International Energy Conference, IEEE, 2010, pp. 820–825, <http://doi.org/10.1109/ENERGYCON.2010.5771795>.
 65. O. Ekren and B. Y. Ekren, “Size optimization of a PV/wind hybrid energy conversion system with battery storage using simulated annealing,” *Appl. Energy*, vol. 87, no. 2, pp. 592–598, 2010, <https://doi.org/10.1016/j.apenergy.2009.05.022>.
 66. O. Ekren and B. Y. Ekren, “Size optimization of a PV/wind hybrid energy conversion system with battery storage using response surface methodology,” *Appl. Energy*, vol. 85, no. 11, pp. 1086–1101, 2008, <https://doi.org/10.1016/j.apenergy.2008.02.016>.
 67. A. Crăciunescu, C. Popescu, M. Popescu, and L. M. Florea, “Stand-alone hybrid wind-photovoltaic power generation systems optimal sizing,” in AIP Conference Proceedings, American Institute of Physics, 2013, pp. 1253–1256, <https://doi.org/10.1063/1.4825738>.
 68. A. K. Kaviani, H. R. Baghaee, and G. H. Riahy, “Optimal sizing of a stand-alone wind/photovoltaic generation unit using particle swarm optimization,” *Simulation*, vol. 85, no. 2, pp. 89–99, 2009, <https://doi.org/10.1177/0037549708101181>.
 69. H. R. Baghaee, M. Mirsalim, G. B. Gharehpetian, and H. A. Talebi, “Reliability/cost-based multi-objective Pareto optimal design of stand-alone wind/PV/FC generation microgrid system,” *Energy*, vol. 115, pp. 1022–1041, 2016, <https://doi.org/10.1016/j.energy.2016.09.007>.
 70. H. R. Baghaee, M. Mirsalim, and G. B. Gharehpetian, “Multi-objective optimal power management and sizing of a reliable wind/PV microgrid with hydrogen energy storage using MOPSO,” *J. Intell. Fuzzy Syst.*, vol. 32, no. 3, pp. 1753–1773, 2017, <http://doi.org/10.3233/JIFS-152372>.
 71. A. Arabali, M. Ghofrani, M. Etezadi-Amoli, and M. S. Fadali, “Stochastic performance assessment and sizing for a hybrid power system of solar/wind/energy storage,” *IEEE Trans. Sustain. Energy*, vol. 5, no. 2, pp. 363–371, 2013, <http://doi.org/10.1109/TSTE.2013.2288083>.
 72. A. M. Jasim, B. H. Jasim, F.-C. Baiceanu, and B.-C. Neagu, “Optimized sizing of energy management system for off-grid hybrid solar/wind/battery/biogasifier/diesel microgrid system,” *Mathematics*, vol. 11, no. 5, p. 1248, 2023, <https://doi.org/10.3390/math11051248>.
 73. M. Kharrich et al., “Developed approach based on equilibrium optimizer for optimal design of hybrid PV/wind/diesel/battery microgrid in Dakhla, Morocco,” *IEEE Access*, vol. 9, pp. 13655–13670, 2021, <http://doi.org/10.1109/ACCESS.2021.3051573>.
 74. A. A. Z. Diab, H. M. Sultan, I. S. Mohamed, O. N. Kuznetsov, and T. D. Do, “Application of different optimization algorithms for optimal sizing of PV/wind/diesel/battery storage stand-alone hybrid microgrid,” *Ieee Access*, vol. 7, pp. 119223–119245,

- 2019, <http://doi.org/10.1109/ACCESS.2019.2936656>.
75. M. Kharrich, L. Abualgah, S. Kamel, H. Abdel-Sattar, and M. Tostado-Véliz, "An Improved Arithmetic Optimization Algorithm for design of a microgrid with energy storage system: Case study of El Kharga Oasis, Egypt," *J. Energy Storage*, vol. 51, p. 104343, 2022, <https://doi.org/10.1016/j.est.2022.104343>.
 76. M. Thirunavukkarasu, Y. Sawle, and H. Lala, "A comprehensive review on optimization of hybrid renewable energy systems using various optimization techniques," *Renew. Sustain. Energy Rev.*, vol. 176, p. 113192, 2023, <https://doi.org/10.1016/j.rser.2023.113192>.
 77. M. Ramesh and R. P. Saini, "Dispatch strategies based performance analysis of a hybrid renewable energy system for a remote rural area in India," *J. Clean. Prod.*, vol. 259, p. 120697, 2020, <https://doi.org/10.1016/j.jclepro.2020.120697>.
 78. A. M. Patel and S. K. Singal, "Optimal component selection of integrated renewable energy system for power generation in stand-alone applications," *Energy*, vol. 175, pp. 481–504, 2019, <https://doi.org/10.1016/j.energy.2019.03.055>.
 79. S. Rajanna and R. P. Saini, "Modeling of integrated renewable energy system for electrification of a remote area in India," *Renew. Energy*, vol. 90, pp. 175–187, 2016, <https://doi.org/10.1016/j.renene.2015.12.067>.
 80. P. Ravibabu, K. Venkatesh, T. Swetha, S. F. Kodad, and B. V. S. Ram, "Application of DSM techniques and renewable energy devices for peak load management," in 2008 IEEE Region 8 International Conference on Computational Technologies in Electrical and Electronics Engineering, IEEE, 2008, pp. 129–132, <http://doi.org/10.1109/SIBIRCON.2008.4602569>.
 81. M. A. Jirdehi and S. Ahmadi, "The optimal energy management in multiple grids: Impact of interconnections between microgrid–nanogrid on the proposed planning by considering the uncertainty of clean energies," *ISA Trans.*, vol. 131, pp. 323–338, 2022, <https://doi.org/10.1016/j.isatra.2022.04.039>.
 82. M. M. Kamal, I. Ashraf, and E. Fernandez, "Planning and optimization of microgrid for rural electrification with integration of renewable energy resources," *J. Energy Storage*, vol. 52, p. 104782, 2022, <https://doi.org/10.1016/j.est.2022.104782>.
 83. Ç. Iris and J. S. L. Lam, "Optimal energy management and operations planning in seaports with smart grid while harnessing renewable energy under uncertainty," *Omega*, vol. 103, p. 102445, 2021, <https://doi.org/10.1016/j.omega.2021.102445>.
 84. A. Khodaei, S. Bahramirad, and M. Shahidehpour, "Microgrid planning under uncertainty," *IEEE Trans. Power Syst.*, vol. 30, no. 5, pp. 2417–2425, 2014, <http://doi.org/10.1109/TPWRS.2014.2361094>.
 85. A. Khanahmadi, M. Mozaffarilegha, M. Manthouri, and R. Ghaffarpour, "A novel economic method of battery modeling in stand-alone renewable energy systems to reduce life cycle costs," *J. Energy Storage*, vol. 44, p. 103422, 2021, <https://doi.org/10.1016/j.est.2021.103422>.
 86. T. Adefarati and R. C. Bansal, "Reliability assessment of distribution system with the integration of renewable distributed generation," *Appl. Energy*, vol. 185, pp. 158–171, 2017, <https://doi.org/10.1016/j.apenergy.2016.10.087>.
 87. T.-H. Yeh and L. Wang, "A study on generator capacity for wind turbines under various tower heights and rated wind speeds using Weibull distribution," *IEEE Trans. Energy Convers.*, vol. 23, no. 2, pp. 592–602, 2008, <https://doi.org/10.1109/TEC.2008.918626>.
 88. W. Turbines-Part, "3: design requirements for offshore wind turbines," *Proc. IEC*, pp. 61400–61403, 2009, <https://doi.org/10.1002/wene.52>.
 89. A. Betz, *Introduction to the theory of flow machines*. Elsevier, 2014, <https://books.google.com/books>.
 90. J. Lepa, E. Kokin, A. Annuk, V. Pöder, and K. Jürjenson, "Wind power stations performance analysis and power output prognosis," *Eng. Rural Dev. Jelgava*, pp. 92–96, 2008, <http://doi.org/29-30.05.2008>.
 91. S. Dawoud, "Techno Economic Evaluation of Hybrid Energy Isolated Micro-Grids for Rural Areas in Four Zones of Egypt," *J. Adv. Eng. Trends*, vol. 41, no. 2, pp. 153–159, 2021., <https://doi.org/10.21608/jaet.2021.39959.1034>.
 92. I. Y. F. Lun and J. C. Lam, "A study of Weibull parameters using long-term wind observations," *Renew. energy*, vol. 20, no. 2, pp. 145–153, 2000, [https://doi.org/10.1016/S0960-1481\(99\)00103-2](https://doi.org/10.1016/S0960-1481(99)00103-2).
 93. A. L. Bakar, C. W. Tan, and K. Y. Lau, "Optimal sizing of an autonomous photovoltaic/wind/battery/diesel generator microgrid using grasshopper optimization algorithm," *Sol. Energy*, vol. 188, pp. 685–696, 2019, <https://doi.org/10.1016/j.solener.2019.06.050>.
 94. A. Chauhan and R. P. Saini, "Discrete harmony search based size optimization of Integrated Renewable Energy System for remote rural areas of Uttarakhand state in India," *Renew. Energy*, vol. 94, pp. 587–604, 2016, <https://doi.org/10.1016/j.renene.2016.03.079>.
 95. R. Belfkira, P. Reghem, J. Raharijaona, G. Barakat, and C. Nichita, "Non linear optimization based design methodology of wind/PV hybrid stand alone system," *Proc. Eur. Assoc. Vis. Eye Res.*, vol. 1, no. 1, pp. 1–7, 2009, <https://doi.org/10.1016/j.renene.2009.13.054>.
 96. M. Eroglu, E. Dursun, S. Sevencan, J. Song, S. Yazici, and O. Kilic, "A mobile renewable house using PV/wind/fuel cell hybrid power system," *Int. J. Hydrogen Energy*, vol. 36, no. 13, pp. 7985–7992, 2011, <https://doi.org/10.1016/j.ijhydene.2011.01.046>.
 97. P. Arun, R. Banerjee, and S. Bandyopadhyay, "Optimum sizing of battery-integrated diesel generator for remote electrification through design-space approach," *Energy*, vol. 33, no. 7, pp. 1155–1168, 2008, <https://doi.org/10.1016/j.energy.2008.02.008>.
 98. A. S. O. Ogunjuyigbe, T. R. Ayodele, and O. A. Akinola, "Optimal allocation and sizing of PV/Wind/Split-diesel/Battery hybrid energy system for minimizing life cycle cost, carbon emission and dump energy of remote residential building," *Appl. Energy*, vol. 171, pp. 153–171, 2016, <https://doi.org/10.1016/j.apenergy.2016.03.051>.
 99. A. M. Eltamaly and M. A. Mohamed, "Optimal sizing and designing of hybrid renewable energy systems in smart grid applications," in *Advances in renewable energies and power technologies*, Elsevier, 2018, pp. 231–313, <https://doi.org/10.1016/B978-0-12-813185-5.00011-5>.
 100. A. Maleki, "Design and optimization of autonomous solar-wind-reverse osmosis desalination systems coupling battery and hydrogen energy storage by an improved bee algorithm," *Desalination*, vol. 435, pp. 221–234, 2018, <https://doi.org/10.1016/j.desal.2017.05.034>.
 101. A. Yamany, M. A. Mohamed, and Y. Mohammed, "Optimal Sizing and Economic Evaluation of Hybrid Photovoltaic/Wind/Battery/Diesel Generation Systems for Autonomous Utilization," *J. Adv. Eng. Trends*, vol. 43, no. 1, pp. 47–65, 2024, <https://doi.org/10.21608/jaet.2022.131727.1147>.
 102. S. Diaf, D. Diaf, M. Belhamel, M. Haddadi, and A. Louche, "A methodology for optimal sizing of autonomous hybrid PV/wind system," *Energy Policy*, vol. 35, no. 11, pp. 5708–5718, 2007, <https://doi.org/10.1016/j.enpol.2007.06.020>.
 103. A. A. Lazou and A. D. Papatsoris, "The economics of photovoltaic stand-alone residential households: a case study for various European and Mediterranean locations," *Sol. Energy Mater. Sol. Cells*, vol. 62, no. 4, pp. 411–427, 2000, [https://doi.org/10.1016/S0927-0248\(00\)00005-2](https://doi.org/10.1016/S0927-0248(00)00005-2).
 104. D. B. Nelson, M. H. Nehrir, and C. Wang, "Unit sizing of stand-alone hybrid wind/PV/fuel cell power generation systems," in *IEEE Power Engineering Society General Meeting*, 2005, IEEE, 2005, pp. 2116–2122, <http://doi.org/10.1109/PES.2005.1489286>.
 105. A. Navaeefard, S. Tafreshi, and M. Maram, "Distributed energy resources capacity determination of a hybrid power system in electricity market," in *25th International Power System Conference*, 2010, <https://doi.org/10.1016/j.rser.2009.10.025>.
 106. A. Kaabeche, M. Belhamel, and R. Ibtouen, "Optimal sizing method for stand-alone hybrid PV/wind power generation system," *Rev. des Energies Renouvelables Bou Ismail Tipaza*, vol. 1, pp. 205–213, 2010, <https://doi.org/10.1116/j.rser.2010.10.015>.
 107. S. P. Ayyeng'o, T. Schirmer, K.-P. Kairies, H. Axelsen, and D. U. Sauer, "Comparison of off-grid power supply systems using lead-acid and lithium-ion batteries," *Sol. Energy*, vol. 162, pp. 140–152, 2018, <https://doi.org/10.1016/j.solener.2017.12.049>.
 108. S. Mirjalili, A. H. Gandomi, S. Z. Mirjalili, S. Saremi, H. Faris, and S. M. Mirjalili, "Salp Swarm Algorithm: A bio-inspired optimizer for engineering design problems," *Adv. Eng. Softw.*, vol. 114, pp. 163–191, 2017, <https://doi.org/10.1016/j.advengsoft.2017.07.002>.

Abbreviation and Symbols

DSM	Demand Side Management.	SMCS	Sequential Monte Carlo Simulation.
LF	Load Following.	CS	Cuckoo Search.
CC	Cycle Charging.	KSA	The Kingdom of Saudi Arabia.
COE	Cost of Generated Energy.	ABC	Artificial Bee Colony.
LPSP	Loss of Power Supply Probability.	IAOA	Improved Arithmetic Optimization Algorithm.
SSA	Salp Swarm Algorithm.	WOA	Optimizer of Whale Optimization Algorithm
RE	Renewable Energy.	WCA	Optimizer of Water Cycle Algorithm
GHGs	Greenhouse Gases.	MFO	Optimizer of Moth Flame Optimizer.
CO ₂	Carbon Dioxide.	GRO	Gray Wolf Optimizer.
HPT	Heat Pumping Technologies	DA	Dragonfly Algorithm.
GH	Green Hydrogen.	ALO	Ant Lion Optimizer.
HP	Hydropower.	NASA	National Aeronautics and Space Administration.
PV	Photovoltaic	H	Height of the Hub.
SHC	Solar Heating and Cooling.	h_a	Height of the Anemometer.
IEA	International Energy Agency.	$u(h)$	The Wind Speed at The Height of The Hub.
IHRES	Integrated Hybrid Renewable Energy System.	$u(h_a)$	The Wind Speed at The Height of The Anemometer.
FC	Fuel Cell.	α	Roughness Factor.
FW	Flywheel.	P_{Load}	The Hourly Demand Load.
HPSS	Hydroelectric Pumped Storage System.	P_{mech}	The Wind Turbine's Mechanical Output Power.
DG	Diesel Generator.	ρ	The Air Density.
WT	Wind Turbine.	A	The Rotor Blade Swept Area (m ²).
RES	Renewable Energy Sources.	C_p	The Power Coefficient for Wind Turbine.
GHI	Global Horizontal Irradiation for Cite.	R	The Turbine Radius (meters).
HRES	Hybrid Renewable Energy System.	ω	The Turbine's Angular Velocity (Rad/Sec).
iHOGA	Improved Hybrid Optimization by Genetic Algor.	λ	The Wind Speed Ratio.
NREL	National Renewable Energy Laboratory.	$cut - in$	The Cut-In Wind Speed.
RERL	Renewable Energy Research Laboratory.	$cut - rated$	The Rated Wind Speed.
HOMER	Hybrid Optimization Model for Electrical Renewable Sources.	$cut - off$	The Cut-Off Wind Speed.
TRNSYS	Transient Energy System Simulation Program.	K	The Shape Parameter.
HVAC	Heating, Ventilation and Air Conditioning.	C	The Scale Parameter.
ISE	Institute of Solar Energy.	$F(u)$	The Cumulative Distribution Function.
MOSADE	Multi-Objective Self-Adaptive Differential Evolution Algorithm.	P_{WT}	The Power Generated from WT.
MBA	Mine Blast Algorithm.	E_{WT}	The Energy Generated from WT.
PICEA	Preference Inspired Coevolutionary Algorithm.	N_{WT}	The Number of WTs.
ANN	Artificial Neural Network.	Δt	Time Interval.
DHS	Discrete Harmony Search.	P_{PV}	The Power Generated From PV
GA	Optimizer of Genetic Algorithm.	E_{PV}	The Energy Generated From PV
PSO	Optimizer of Particle Swarm Optimization.	N_{PV}	The Number of PV Panels.
SAA	Optimizer of Simulated Annealing Algorithm.	Δt	The Time Interval.
RSM	Response Surface Methodology.	P_{Load}	The Demand Load Power.
MOPSO	Optimizer of Multi-Objective Particle Swarm Optimization.	P_{Gen}	The Total Electrical Power Generated.
COE	Cost of Energy.	σ	The Hourly Self-Discharge Rate.
		P_{BC}	The Battery Charging Power.
		P_{BD}	The Battery Discharging Power.
		E_{Bat}	The Energy That Is Stored in The Battery Bank

N_{Bat}	Number of Battery Cells.
η_{Conv}	The Bi-Directional Converter Efficiency.
η_{BC}	The Battery Charging Efficiency.
η_{BD}	The Battery Discharging Efficiency.
E_{Bat_max}	The Maximum Allowable of Battery Storage Capacity.
E_{Bat_min}	The Minimum Allowable of Battery Storage Capacity.
DOD	Depth of Discharge of The Storage Battery.
C_{Bat}	The Battery Storage Nominal Capacity.
F_{DG}	The DG Hourly Fuel Consumption.
a_{DG} and b_{DG}	The Operating Coefficients.
P_{DG_Gen}	The Hourly Produced Power
P_{DG_rating}	The Rated Power of the DG
F_{DG}	The Fuel Consumption Per Hour of the DG.
AFC	The DG Annual Fuel Consumption.
$CO_2(t)$	The Hourly Emissions Per Liter.
BDC-CC	Bidirectional Converter with A Charge Controller
EMS	Energy Management Strategy.
LCC	Life Cycle Cost.
TPC	The Total Present Cost of The Overall Project.
LAE	The Annual Required Load.
CRF	The Capital Recovery Factor.
T	The Project Lifetime in Years.
y	The Discount Rate
i_{nom}	The Real Net Interest Rate.
f	The Annual Inflation Rate.
$C_{Initial_Capital}$	The Initial Capital Cost.
C_{PV}	Cost of PV System Including Civil Works Per Kw.
C_{WT}	Cost of WT Including Civil Works Per Kw.
C_{Bat}	The Cost of Battery Storage Per Kwh.
P_{BDC-CC}	The Rated Power of The Converter.
C_{BDC-CC}	The Cost of Converter Per Kw.
C_{DG}	The Cost of DG Per Kw.
$C_{O\&M}$	The Operation and Maintenance Cost.
C_{Rep}	The Replacement Cost.
C_{Fuel}	The Fuel Cost of DG.
P_{Fuel}	The Price of Fuel Per Liter.
V_{Scarp}	The Scrap Present Value.
E_{Dump}	The Energy of Dump Load.
P_{Dump}	The Power of Dump Load.
t	Time.